MSc Thesis:

Structural Response of the Bjornefjord Submerged Floating Tunnel in current flow

Delft University of Technology

Offshore and Dredging Engineering MSc Programme

Faculty of Mechanical Engineering and Marine Technology, Civil Engineering

September 2019

Student:	Papadopoulos Giorgos	*Committee:*	Prof.Dr. A.Metrikine — TU Delft - Chairman
			Dr.Ir. K.N.van Dalen — TU Delft - Asst. Prof.
			Dr. Joao Barbosa — TU Delft - Researcher
			Dr. Richard Ogink — TU Delft - Researcher

Acknowledgements

Throughout the writing of the present Master thesis report I have received a great deal of support and it would be a serious omission not to acknowledge the guidance and assistance of specific people and to express my deepest gratitude.

First and foremost, I would like to thank my supervisor, Joao Barbosa, for being such a great guide and such an awesome person. Whenever I had doubts and seeking for help, he was always there, providing necessary guidance and support. I completely enjoyed working with you these last 10 months, I learnt so many new things and had a great time throughout our long conversations.

Furthermore, I want to express my gratitude to professor Andrei Metrikine, for giving me the foundations on which to grow and on which to build, that will accompany me for the rest of my life. I would also like to thank Richard Ogink for his valuable ideas and propositions through the progression of the thesis, as well as his enthusiasm towards my project.

Nothing could have been possible without specific people behind me, constantly supporting my effort and purpose. No words can express my gratitude to my family and friends. The highest appreciation is to not utter words, but live by them.

Giorgos Papadopoulos
Delft, September 2019

Summary

The Submerged Floating Tunnel (SFT) is an innovative type of transport structure, with significant advantages in crossing long, deep and wide water areas, compared to more conventional types of bridges. Recognizing its potential, the Norwegian Public Roads Administration is planning to use such technology, in creating a ferry-free highway that will connect the west coast of Norway.

The objective of the present Master thesis report is to develop a model on a tether-stabilized SFT and investigate the static and dynamic load effects acting on such a structure in order to estimate how safe can such a structure be. The modeling of the SFT has been based on prototype designs, specifically developed for Bjornefjord in Norway. Focus has been put on capturing the Vortex-Induced Vibrations generated on the structure, when interacting with a current flow. Matlab has been used to describe the SFT and solve the dynamic problem. Facchinetti's wake oscillator model is applied to couple the tunnel motions with the vortex shedding. In the present report, the tether motions are not taken into account and, conservatively, tethers are modeled as springs.

The 100-year current speed was used to excite the structure and it was found that the SFT is not influenced significantly. An SFT configuration with a free-span length of *210m*, between two consecutive tethers along the total length, is capable enough to dissolve any VIV effects. Only when a free-span length of *700m* is used, vibrations in the cross-flow direction make their presence felt. A simple estimation of the 100-year swell wave force was also performed, showing similar forcing magnitudes as the current force with an excitation frequency much closer to the 1st natural frequency of the structure. This renders the structure a lot more sensitive. Furthermore, the effect of an unexpected tether failure was investigated and showed that the system can safely reach to a new equilibrium position, without any progressive damage. Overall, despite all the hesitation around this concept, it has proven to be quite promising.

Contents

1 Introduction

A submerged floating tunnel (SFT) is a proposed concept of an immersed tube, that floats in water, used to cross straits or other long deep water areas. The tube is placed at a water depth of approximately 30 m, deep enough to avoid water traffic and weather conditions at the surface, but shallow enough to deal with water pressures. It is anchored mainly by tethers connected to the seafloor or by pontoons at the surface, as depicted in Figure 1.1.
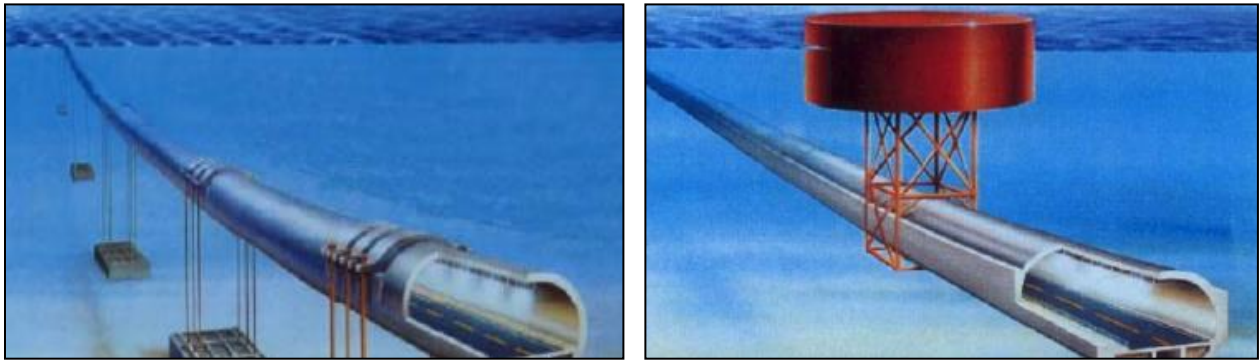

Figure 1.1: Typical SFT restrained by a. tethers, b. pontoons

1.1 Motivation

The concept of an underwater floating tunnel originated in the 1886, when the first patent was granted. Ever since, multiple concept proposals have come up, but none of these ideas has taken actual shape, as of 2019. A submerged floating tunnel (SFT) allows the construction of a "bridge" in extremely deep water, where other conventional concepts would be unreasonably expensive. Due to its potential, the interest on constructing such a structure was revived recently more relevant than ever, with possible sites of application all over the world. Norway's efforts on connecting all its western fjord crossings and eliminating the use of ferry boats (European route E39) stands out as a potential application of the SFT concept. Other countries that have expressed interest in this new technology are China, Japan and Italy.

1.2 Objective/Scope

The objective of the present thesis is to provide an insight on how safe can an SFT be, under certain environmental conditions, present in situ. For this purpose, the response of the SFT under current and wave loading is investigated, emphasizing on the effect of vortex induced vibrations (VIV) on the tunnel. A challenging design has been developed for Bjornefjord in Norway, based on a prototype design from a study conducted by *Reinertsen, Olav Olsen & Norconsult Group*[1]. In the present report, pontoon stabilized SFT's are not considered and configurations with tether based supporting are investigated. Multiple tunnel-tether designs are tested, in order to predict motion amplifications and evaluate safety. For the external excitations, both the 100 year return period current and wave are used, providing

---

[1] This partnership has been commissioned the study by the Norwegian Public Road Administration (NPRA).

valuable information for the corresponding environmental loads. Lastly, the probability of a successive tether failure, when one tether unexpectedly fails, possibly due to a foundation failure or fatigue damage, is modeled and investigated. How the new structural configuration will react to such an unexpected effect, is of importance for the human safety.

1.3 Advantages and Design Challenges

A submerged floating tunnel offers many advantages, which explains why lots of nations are oriented towards constructing one in the future. Compared to more conventional 'bridge' concepts, depicted in Figure 1.2, the advantages of an SFT are:

- The length of an SFT (concept 2) is significantly shorter than from an immersed tube (concept 3) or an underground tunnel (concept 4), leading to significantly lower structural/material expenses
- When having to connect two lands with long distance in between, a bridge (concept 1) is difficult to be built
- It is not affected by the water surface environmental conditions nor by the wind conditions
- The design of an SFT is not influenced by the water depth
- It is considered to be economically advantageous, as the cost per unit length of an SFT is not affected by the total length of the structure, compared to a bridge for instance
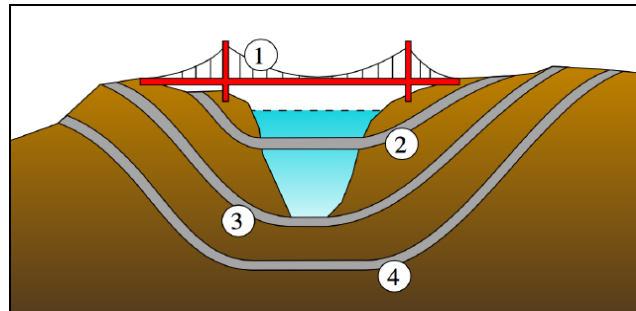

Figure 1.2: Different types of 'bridges', 1) Conventional bridge, 2) SFT, 3) Immersed tunnel, 4) Underground tunnel

Concerning the challenges when designing an SFT, structure stability is one of the most decisive parameters. Stability of an SFT is crucial and depends on the dead weight, the buoyancy, the pre-tension on the tethers and the external excitation. More troubling challenges that engineers need to account for when designing an SFT are:

- Understanding the effect of current and wave loading on the tube is quite complex, and not many experiments have been performed to support research. The uncertainty behind fluid-structure interaction is a huge difficulty an engineer needs to overcome
- Oceanic environments are unfriendly and harsh. Corrosion, fatigue damage, collision accidents are parameters that need to be taken into account

- As none similar project has been built before, there are lots of risks and uncertainties related to the construction, installation and operation phase. Getting into murky waters always feels uncomfortable

1.4 Existing literature

The SFT is designed to operate in a complex marine environment. Researchers have devoted their efforts on capturing the dynamic behavior of the SFT under hydrodynamic excitations. Based on the existing theory it is expected that VIV's will occur on the SFT and the anchor tethers, by the action of vortex shedding. When the shedding frequency becomes close to the natural frequency of the structure, large and damaging oscillations take place, a condition named 'lock-in'. Paik et al. (1) developed a finite element model to explore the dynamic response of an SFT to wave loads, focusing on the effect of the SFT depth on the dynamic behavior. Mazzolani et al. (2) studied both the static and the dynamic response of an SFT under wave loading, in search of the best performing cable-tunnel configuration in view of a seismic analysis and Hiroshi Kunisu (3) did something similar with different anchorage types. Long et al. (4) studied the effects of some basic structure parameters on the dynamic response under waves and current. Xiang et al. (5) coupled the nonlinear vibrations of both the anchored tethers and the tube, based on the Hamilton principle and the Morison equation. Overall, extensive attention has been drawn on the hydrodynamic behavior of an SFT, as being the most decisive parameter.

The tunnel's dynamic response is the primary objective in the present report as well. In contrast to other works, the torsional motion of the tube has been acknowledged, a component that largely contributes to the in-line motion of the SFT. The anchor cables are modeled as springs, providing the necessary support stiffness. This means that the effect of tether vibrations on the tunnel motion is ignored. The Van der Pol wake oscillator model has been used to couple the wake behind the cylinder and the tunnel motions when dealing with current loading. The present FE model is established to evaluate the effect of specific structure's parameters and reach to a best performing configuration.

2 Current flow on oscillating cylinder

2.1 Concept Description, dimensions & materials

An FE model has been specifically designed for the Bjornefjord, a Norwegian fjord, potential site for installation of an SFT, for the needs of the European route E39. It is based on previous studies and designs, conducted by a partnership of Norwegian companies and research groups. The SFT is located 30 m below the water surface and it has been assumed that a constant water gap of 30 m exists between the tube and the mudline, along the length of the tunnel. This means that Bjornefjord has water depths down to about 60 m, which is a simplification given the bathymetry on site (6).

The original concept, named as the 'prototype design', has two tubes connected together to form the two lane highway. In the present report only one tube, instead of two, is considered, deviating from the prototype design. This is done purely to simplify the modeling in Matlab. Figure 2.1 shows the tunnel-tether configuration with $L=L_1+L_2+...+L_N$ the total length of the tunnel[2] with diameter D. Angle α defines where the connection of the tether with the tube is happening and is formed by the radius going through the tunnel-tether connection point and the horizontal line and angle β the one formed by the tether and the mudline. Direction x is the horizontal direction in-line with the flow, direction y the transverse motion direction and z the longitudinal direction of the tunnel.
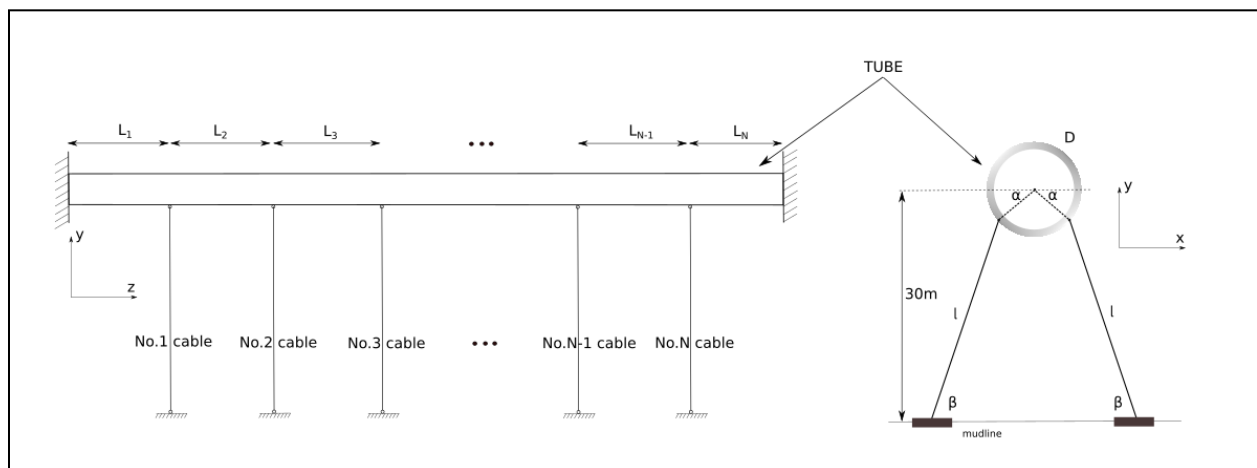

Figure 2.1: Tunnel - Tether configuration

The tunnel has a total length of 5500 m. The prototype design has been designed with vertical tethers and with a curved alignment to add the necessary horizontal support stiffness. This will oppose flows coming from the Atlantic ocean. In the developed model, the tunnel is considered as a straight line. For this reason, tethers under an angle are used to restrain the tunnel's horizontal motion. Key parameters of the tunnel's dimensions are shown at Table 2.1.

---

[2] Multiple tunnel segments, of equal length, form the total 5500 m tube

Parameter	Unit	Magnitude
Length	M	5500
Outer diameter	M	15
Thickness	M	0.8
Cross sectional area	m^2	42.1
Second moment of inertia	m^4	902.4
Polar moment of inertia	m^4	1804.8
Depth	M	30
Mass	ton/m	133.08

Table 2.1: Dimensional properties of the main tube

As mentioned, mooring tethers, under an angle *β*, are used to restrain the motion of the tunnel in the *x* and *y* directions. Two tethers are used in each segment of the tunnel, symmetrically positioned. A total of 25 tether pairs have been used throughout the total length of the tunnel, one pair every 210 m according to the original design. The tube floats underwater, meaning that it has a positive net buoyancy; the structure has a 0.92 mass ratio, which expresses the ratio of the structural mass divided by the mass of the displaced water. This results in tether pre-tension, which must comply also with acceptable values. According to von Schack (7), the tether pre-tension shouldn't exceed 1/3 of the resistance, resulting in an allowable tension of ≈9 MN.

Parameter	Unit	Magnitude
No. of tether pairs	-	25
Outer diameter	M	1.118
Thickness	M	0.038
Cross sectional area	m^2	0.13
Nominal pre-tension	MN	9.04
Mass	ton/m	1.012

Table 2.2: Dimensional properties of the tethers

The material used for the tube is concrete grade B55 M40, and for the tethers steel S235, as in Table 2.3.

Parameter	Unit	Concrete B55 M40	Steel S235
Modulus of elasticity	GPa	30	207
Shear modulus	GPa	12.5	80
Density	kg/m³	3160.06	7850
Yield strength	MPa	-	235
Tensile strength	Mpa	3	-

Table 2.3: Material properties

2.2 Vortex Induced Vibrations

The phenomenon of vortex shedding behind a circular cylinder is well understood by the engineers. When the flow layer, closer to the cylinder boundaries, separate from the body, vortices are formed. These vortices change the pressure distribution around the cylinder walls, as depicted in Figure 2.2, creating some force components in the vertical direction, leading to cylinder oscillations transverse to the flow direction.
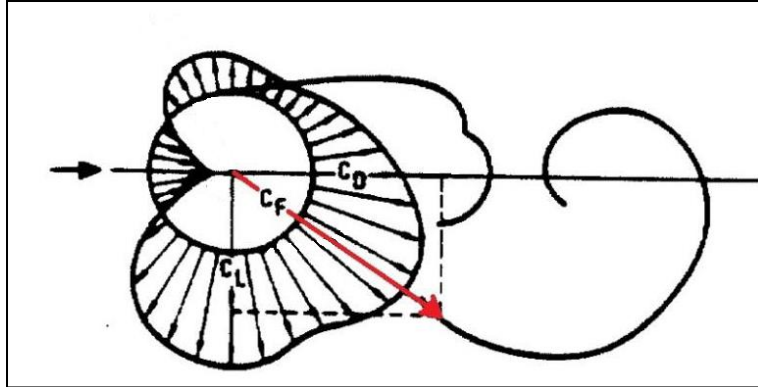
Figure 2.2: Near wake pressure distribution

The frequency at which vortices are shedded is called Strouhal frequency, and under certain conditions is proportional to the flow velocity and inversely proportional to the cylinder diameter.

$$f_s = \frac{U \cdot St}{D}$$

The Strouhal number *St* depends on the Reynolds number, as shown in Figure 2.3. For a rough surface cylinder (concrete cylinder), a constant Strouhal value of 0.2 for Reynolds numbers till 10^6 is a good estimation. Thus, the vortex shedding frequency is linearly proportional to the flow velocity. When the Strouhal frequency comes close to the natural frequency of the structure, the amplitude of oscillation locks in large values, that can damage the structure. Khalak and Williamson (8) studied the response of a cylinder over a range of current velocities and described the lock-in phenomenon quite extensively for low mass-damping systems. Figure 2.4 summarizes the results of their research. For small values of the reduced velocity[3] the vibration amplitudes are insignificant. When the reduced velocity reaches a specific value, which depends on the systems mass ratio, the shedding frequency becomes equal to the natural frequency of the system entering the synchronization range (upper branch). This is when lock-in occurs and large amplitude oscillations take place. The lock-in range extends for even larger reduced velocities, entering the lower branch region. The shedding frequency remains constant and equal to the vibration frequency of the system, in contrast to what the Strouhal equation predicts, for increased reduced velocity. At some point, the vibration amplitude decreases rapidly and VIV's are no longer present. At that point the shedding frequency unlocks from the systems vibration frequency.

---

[3] Reduced velocity is defined as the current velocity normalized by the excitation frequency and the cylinder diameter $V_r = \frac{V}{f_{st}D}$
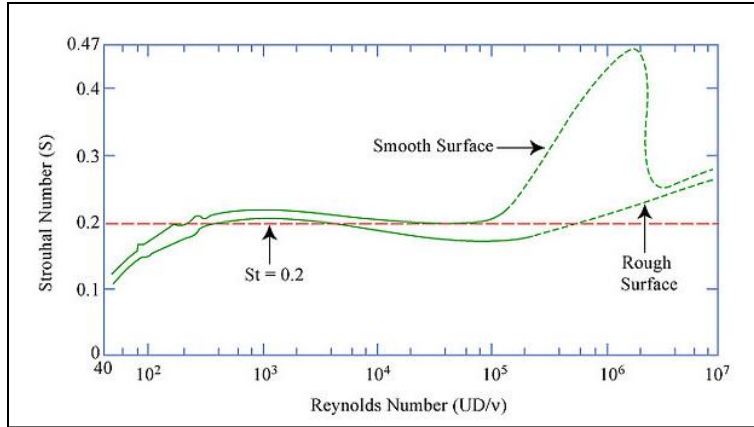
Figure 2.3: Relation between Reynolds number and Strouhal number (Lienhard 1966)
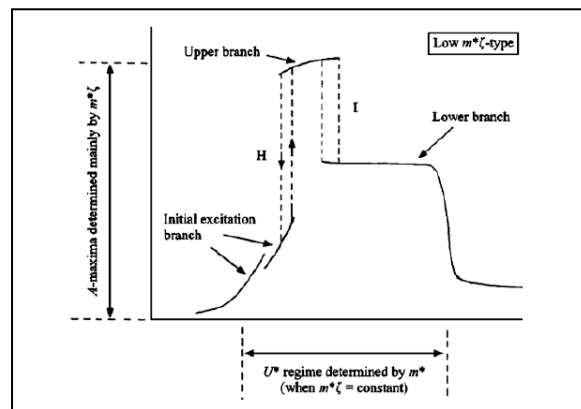

Figure 2.4: Maximum response amplitude wrt the reduced velocity

2.3   Equations of Motion

The tunnel's dynamic response is investigated, under a current flow excitation. Later on, the influence of the wave loads will also be investigated in contrast to the current load. The structure experiences in-line and cross flow vibrations, in the **x** and **y** directions, and is subjected to forces F_x and F_y, created by a current flow coming under an angle φ and a constant velocity V (Figure 2.5).
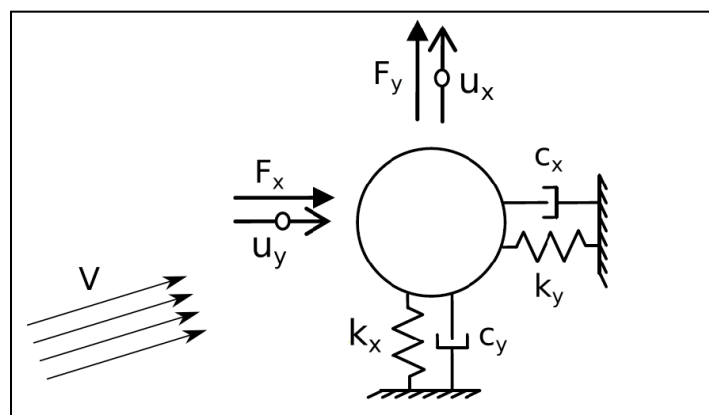
Modeling the tunnel as a sequence of beam elements allows for a good description of the motions. The equations that describe the motion of the tunnel are (longitudinal deflection in the **z** direction is ignored):

In-line:
$$(m + m_a)\frac{\partial^2 u_x(z,t)}{\partial t^2} + c_x \frac{\partial u_x(z,t)}{\partial t} + EI \frac{\partial^4 u_x(z,t)}{\partial z^4} - T \frac{\partial^2 u_x(z,t)}{\partial z^2} = F_x$$

Cross flow:
$$(m + m_a)\frac{\partial^2 u_y(z,t)}{\partial t^2} + c_y \frac{\partial u_y(z,t)}{\partial t} + EI \frac{\partial^4 u_y(z,t)}{\partial z^4} - T \frac{\partial^2 u_y(z,t)}{\partial z^2} = F_y$$

with the axial tension T being ignored. In order to estimate the forces acting on the cylinder from the current flow, a forced Van der Pol wake oscillator model is used with acceleration coupling, based on Facchinetti (9). It is an empirical model, that uses parameter q to describe the coupling between the wake behind the rigid cylinder and the forces on the cylinder. When the cylinder starts to vibrate, it disturbs the flow pattern, consequently, changing the lift force that was causing the cross flow vibrations. Change in the lift force will cause a change in the vibration amplitude, which will again modify the flow around the cylinder, until a steady state is reached. The differential equation is as follows:

$$\ddot{q} + \varepsilon\omega_s(q^2 - 1)\dot{q} + \omega_{st}^2 q = \frac{A}{D}\left(\frac{\partial^2 y(z,t)}{\partial t^2}cos\varphi - \frac{\partial^2 x(z,t)}{\partial t^2}sin\varphi\right)$$

Parameters ε and A are tuning parameters, that are found based on existing experiments. It has been found that they are strongly influenced by the mass-damping system characteristics (8). Variable ω_s is the shedding frequency and is based on the flow velocity. For the forcing term in the wake oscillator equation, acceleration coupling has been chosen, as it has been assumed that it captures the lock-in region more efficiently than other types of coupling (9).

The external forcing terms in the motion equations are coming from a drag component, in line with the relative velocity of the cylinder, and a lift component, perpendicular to the drag force. The drag force is assumed to be proportional to the square of the relative velocity, with a drag coefficient C_{D0}. The lift force is on the other hand proportional to the wake parameter q. Decomposing the in-line and cross flow force components into the **x** and **y** directions, the following expressions for F_x and F_y are obtained:

$$F_x = \frac{1}{2}\rho D\left(C_{D0}\left(V_x - \frac{\partial x(z,t)}{\partial t}\right) + \frac{C_{L0}}{2}q\left(V_y - \frac{\partial y(z,t)}{\partial t}\right)\right)\sqrt{\left(V_x - \frac{\partial x(z,t)}{\partial t}\right)^2 + \left(V_y - \frac{\partial y(z,t)}{\partial t}\right)^2}$$

$$F_y = \frac{1}{2}\rho D \left(C_{D0}\left(V_y - \frac{\partial y(z,t)}{\partial t}\right) + \frac{C_{L0}}{2}q\left(V_x - \frac{\partial x(z,t)}{\partial t}\right)\right)\sqrt{\left(V_x - \frac{\partial x(z,t)}{\partial t}\right)^2 + \left(V_y - \frac{\partial y(z,t)}{\partial t}\right)^2}$$

V_x and V_y are the horizontal and vertical components of the current speed, which is assumed to be constant along the total length of the tunnel, in **z** direction. The three differential equations are solved using a Runge-Kutta fourth order method.

2.4 Environmental Conditions on site

Unfortunately, for the support of this report, there are no in-situ environmental data available. Therefore, design values for the significant wave height and the spectral peak period are taken from the Reinertsen et al. (6).

2.4.1 Current

The 100 year return period for the current speed, as well as the 10000 year return period, can be found in Table 2.4. According to the current speed at surface, and using a linear interpolation based on scale values, the current at any water depth can be found.

Return period [year]	1	10	50	100	10000
Current speed in surface [m/s]	0.5	0.6	0.65	0.7	0.9
Current speed at tube depth [m/s]	0.19	0.23	0.25	0.27	0.34

Table 2.4: Current velocities at tube depth

2.4.2 Wind & Swell waves

The Norwegian Public Road Administration (NPRA), which is involved in the design of the SFT project, has defined the design values for the 100 year wind-sea and swell waves to be used.

Hs [m]	Tp [s]	γ	Direction [deg]
3	6	3.2	270

Table 2.5: 100y wind-sea design values

Hs [m]	Tp [s]	γ	Direction [deg]
0.3	14	5	300

Table 2.6: 100y swell design values

Based on the Airy wave theory and using the design values specified above, the wave profiles are plotted with respect to the water depth, in Figure 2.6. It becomes evident that wind-sea waves are of non-importance at a water depth of -30 m, where the tube is installed. The impact that swell waves of $H_s = 0.2\ m$ and $T_p = 14\ s$ will have on the structure, on the other hand, can not be neglected and, therefore, will be taken into account.
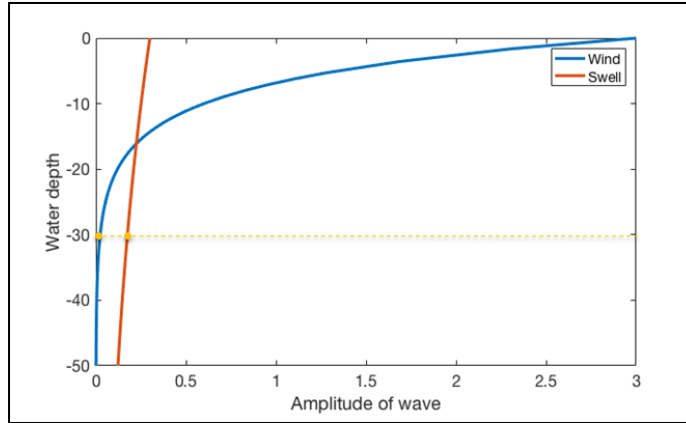
Figure 2.6: Wave profiles in Bjornefjord

3 Tunnel - Tether Configuration

As mentioned in the concept description in §2.1, the curvature of the prototype design is ignored. This curvature was opposing the tunnel motion in the direction of the current flow. Therefore a set of tether angles is defined that will provide the necessary horizontal stiffness. This set of angles is consists of angle α and β as shown in Figure 3.1. A proper selection of these angles can lead to comparatively small tunnel deflections, similar to the prototype design

Although the term 'small deflections' by itself is abstract and there is not much guidance on acceptable SFT deflections from the standard codes, an attempt to comply with the prototype design deflections for a static analysis has been made (6). The initial idea was to use the configuration with the smallest tunnel deflection. As it will be explained later on, this is not feasible and compromises need to be made.
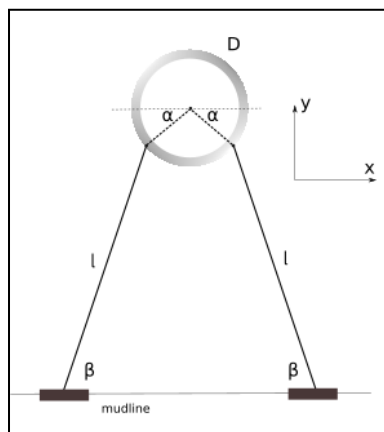

Figure 3.1: Connection point angle α and Tether-Mudline angle β

3.1 Sensitivity analysis of tether angles on a 2D static analysis

The system's response depends, primarily, on the tether angle β with the mudline. This angle defines the horizontal and the vertical stiffness provided by the tethers. Subsequently, the connection point angle α around the tunnel's perimeter influences the rotation of the cylinder. For different values of α and β, the response of the tunnel, to an external forcing, will vary. This motion variation is captured, with the use of a 2D static analysis. The model is excited with a constant drag force, generated by a current flow of *1 m/s* current speed[4].

The tethers are modeled as extension springs. The structure is designed with a positive net buoyancy, for the structure to float. The pre-tension on the tethers, that strongly influences the stiffness of the tether, is calculated based on the net buoyancy of the cross-section:

---

[4] *The 100 year return period current speed, at the Bjornefjord location, is 0.7m/s in surface and 0.27m/s at -30 m water depth. The use of 1 m/s is to add some sort of conservatism in the design.*

$$T = \frac{Buoyancy - Weight}{2sin\beta} \ [N/m]$$

At this point, it was considered wise to apply two different approaches for the tether modeling, as it was unclear how accurate each approach is. Therefore, two different cases of springs were considered, one with constant spring stiffness (linear case), with respect to the tunnel motion, based on the initially calculated tension, and the other one with varying stiffness (non-linear case), based on the change of tether tension, according to the tunnel deflection. The bending stiffness of the tether is not taken into account, as it is considered significantly smaller than the transverse stiffness provided by the tension. Comparing the two cases will show how significant the non-linearity of the tethers is.

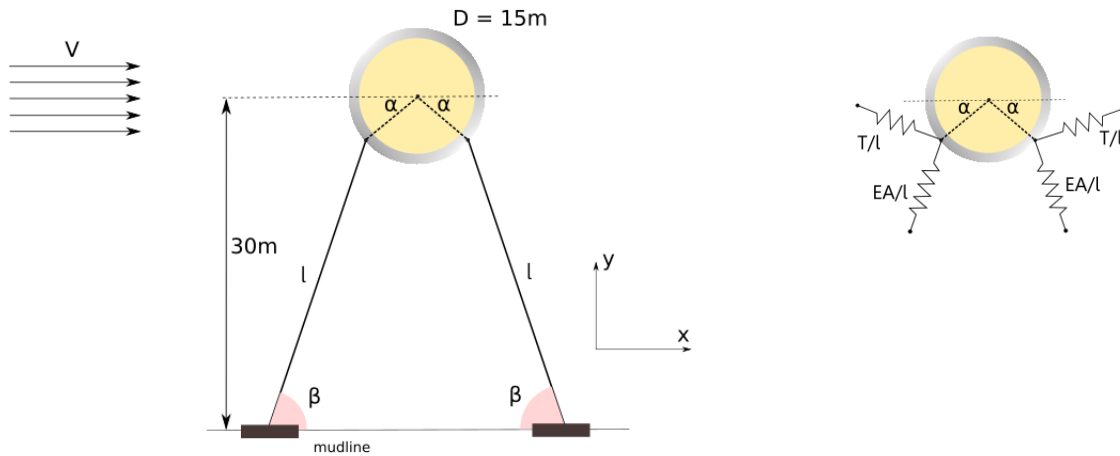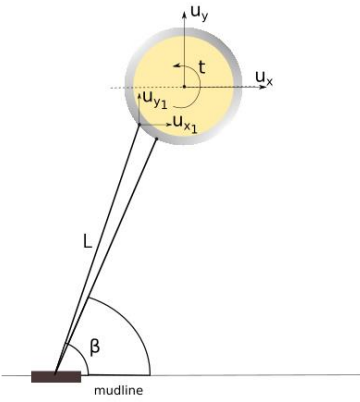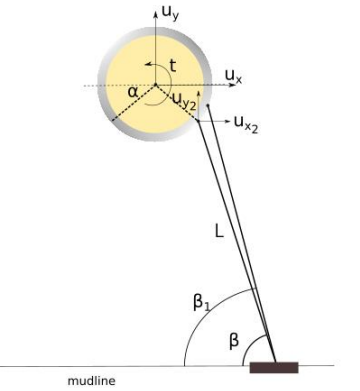## 3.2 Tethers as linear springs

Figure 3.2: a) Plane representation of SFT with tethers, b) Equivalent normal and transverse springs

In the linear case, the system is excited in all three degrees of freedom, namely u_x, u_y, t with a unit amplitude displacement. Based on the procedure followed in Table 3.1, the tether elongation is calculated, according to the positional change of the two connection points, where the tether forces are applied on the tube. Knowing the tether elongation, the forces and moments acting on the tube are can be found. As it was expected, the forces end up being a linear combination of the displacements, with angle β assumed to stay constant.

Left side (Upstream tether) Displacements of contact point $u_{x1} = u_x + t \cdot D/2 \cdot \sin\alpha$ $u_{y1} = u_y - t \cdot D/2 \cdot \cos\alpha$ Extension and force of normal springs $e_{n1} = u_{x1} \cdot \cos\beta + u_{y1} \cdot \sin\beta$ $F_{n1} = -e_{n1} \cdot K_{nt}$ Extension and force of transverse spring $e_{t1} = u_{x1} \cdot \sin\beta - u_{y1} \cdot \cos\beta$ $F_{t1} = -e_{t1} \cdot K_{tt}$ Total forces and moments due to left tether $F_{x1} = F_{n1} \cdot \cos\beta + F_{t1} \cdot \sin\beta$ $F_{y1} = F_{n1} \cdot \sin\beta - F_{t1} \cdot \cos\beta$ $M_1 = F_{x1} \cdot D/2 * \sin\alpha - F_{y1} \cdot D/2 \cdot \cos\alpha$	
Right side (Downstream tether) Displacements contact point $u_{x2} = u_x + t \cdot D/2 \cdot \sin\alpha$ $u_{y2} = u_y + t \cdot D/2 \cdot \cos\alpha$ Extension and force of normal springs $e_{n2} = -u_{x2} \cdot \cos\beta + u_{y2} \cdot \sin\beta$ $F_{n2} = -e_{n2} \cdot K_{nt}$ Extension and force of transverse spring $e_{t2} = -u_{x2} \cdot \sin\beta - u_{y2} \cdot \cos\beta$ $F_{t2} = -e_{t2} \cdot K_{tt}$ Total forces and moments due to right tether $F_{x2} = -F_{n2} \cdot \cos\beta - F_{t2} \cdot \sin\beta$ $F_{y2} = F_{n2} \cdot \sin\beta - F_{t2} \cdot \cos\beta$ $M_2 = F_{x2} \cdot D/2 \cdot \sin\alpha + F_{y2} \cdot D/2 \cdot \cos\alpha$	
Total forces acting on the tube $F_x = F_{x1} + F_{x2} - K_x \cdot u_x$ $F_y = F_{y1} + F_{y2} - K_y \cdot u_y$ $M = M_1 + M_2 - K_t \cdot t$	

Table 3.1: Calculation of the system's stiffness - linear case

Due to the nature of the design, the horizontal and rotational motion of the tunnel are coupled together, whereas the vertical motion of the tunnel is independent of the other two. This means that if one excites the structure horizontally, a rotational motion will also occur. Writing the stiffness into a matrix formation one finds:

$$K = \begin{bmatrix} dF_x/dx & dF_x/dy & dF_x/dt \\ dF_y/dx & dF_y/dy & dF_y/dt \\ dM/dx & dM/dy & dM/dt \end{bmatrix} = \begin{bmatrix} K_{xx} & 0 & K_{xt} \\ 0 & K_{yy} & 0 \\ K_{tx} & 0 & K_{tt} \end{bmatrix}$$

where,

$$K_{xx} = 2K_n cos^2\beta + 2K_t sin^2\beta$$

$$K_{xt} = K_n D cos\beta(cos\beta sin\alpha - cos\alpha sin\beta) + K_t D sin\beta(cos\alpha cos\beta + sin\alpha sinb)$$

$$K_{yy} = 2K_n sin^2\beta + 2K_t cos^2\beta$$

$$K_{tx} = K_{xt}$$

$$K_{tt} = \frac{D^2}{2} cos\alpha\big(K_t cos\beta(cos\alpha cos\beta - sin\alpha sin\beta) + K_n sin\beta(cos\alpha sin\beta - cos\beta sin\alpha)\big)$$

$$- \frac{D^2}{2} sin\alpha\big(K_n cos\beta(cos\alpha sin\beta - sin\alpha cos\beta) - K_n sin\beta(cos\alpha cos\beta + sin\alpha sin\beta)\big)$$

Now that the stiffness of the tethers is known, one can estimate the tunnel motions by solving the Hooke's equation and using a constant drag component equal to $\frac{1}{2}c_{D0}\rho DSV^2$ as the external excitation, with S being the free-span between two consecutive tethers on the three dimensional concept. Results will be included later on in comparison with the non-linear case.

3.3 Tethers as non-linear springs

In the non-linear case the tether is modeled as a rotating spring, meaning that the tension of the tether is always in-line with the tether. The stiffness is not considered constant in this case, but continuously changing value based on the tension. This means that in every analysis iteration, a new stiffness matrix is calculated, based on the positional change of the connection point described in Table 3.2.

Unstretched length (without pretension of tethers)   L = EA·L$_o$/(T+EA)   Relative position of fixed edge to contact points   x$_o$ = L$_o$·cosβ$_o$ y$_o$ = L$_o$·sinβ$_o$

Motion of left contact point Displacements u$_{x1}$ = u$_x$ + D/2·(-cos(α$_o$+t)+cosα$_o$) u$_{y1}$ = u$_y$ + D/2·(-sin(α$_o$+t)+sinα$_o$) Total extension L$_{f1}$ = sqrt((x$_o$+u$_{x1}$)^2+(y$_o$+u$_{y1}$)^2) e$_{n1}$ = (L$_{f1}$-L)/L F$_1$ = -e$_{n1}$·EA β$_1$ = acos((x$_o$+u$_{x1}$)/L$_{f1}$) F$_{x1}$ = F$_1$·cosβ$_1$ F$_{y1}$ = F$_1$·sinβ$_1$ M$_1$ = F$_{x1}$·D/2·sin(α$_o$+t) - F$_{y1}$·D/2·cos(α$_o$+t)	

|	
Motion of right contact point Displacements $u_{x2} = u_x + D/2 \cdot (\cos(\alpha_o\text{-}t)\text{-}\cos(\alpha_o))$ $u_{y2} = u_y + D/2 \cdot (\text{-}\sin(\alpha_o\text{-}t)+\sin(\alpha_o))$ Total extension $L_{f2} = \text{sqrt}((x_o\text{-}u_{x2})^2+(y_o+u_{y2})^2)$ $e_{n2} = (L_{f2}\text{-}L)/L$ $F_2 = \text{-}e_{n2} \cdot EA$ $\beta_2 = a\cos((x_o\text{-}u_{x2})/L_{f2})$ $F_{x2} = \text{-}F_2 \cdot \cos\beta_2$ $F_{y2} = F_2 \cdot \sin\beta_2$ $M_2 = F_{x2} \cdot D/2 \cdot \sin(\alpha_o\text{-}t)+F_{y2} \cdot D/2 \cdot \cos(\alpha_o\text{-}t)$	
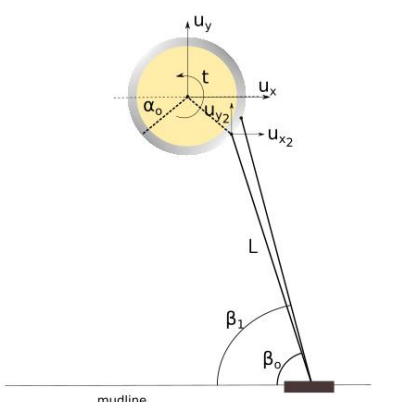
Total forces - Tangent stiffness

$F_x = F_{x1} + F_{x2} + \text{Drag}$

$F_y = F_{y1} + F_{y2} + B$

$M = M_1 + M_2$

$$K_t = \begin{bmatrix} dF_x/du_x & dF_x/du_y & dF_x/dt \\ dF_y/du_x & dF_y/du_y & dF_y/dt \\ dM/du_x & dM/du_y & dM/dt \end{bmatrix}$$

Table 3.2: Calculation of the system's stiffness - non-linear case

3.4 Tether angle effect on the tube's horizontal displacement

3.4.1 Comparative results

In order to find an optimum pair of angles, each angle was tested through a range of possible values. Angle α can vary from 0° to 85°, while angle β from 45° till 120°, as shown in Figure 3.3. Having run the static analysis for all the possible combinations of α and β angles, the output of interest is the horizontal deflection of the cylinder. This is shown in Figure 3.4. At first glance, the results seem to be extremely different. This is because the linear case model is unable to capture, properly, the motion of the tunnel when α angles reach values close to 90°, resulting in an amplification of motions. On the other hand, the non-linear approach seems to predict a more consistent response throughout the angle spans.
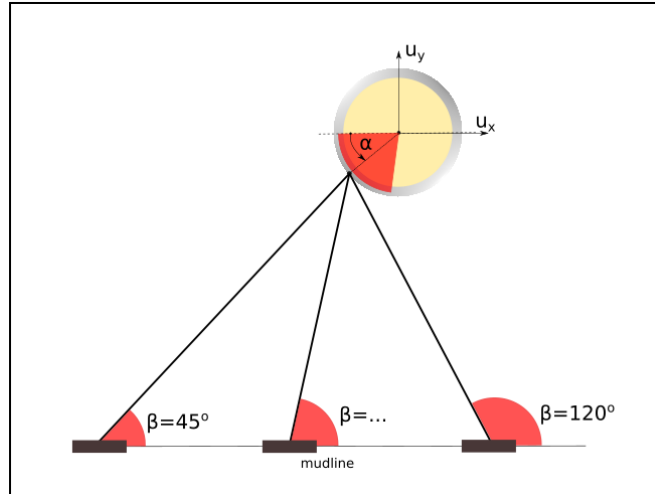
Figure 3.3: Possible α and β angle combinations
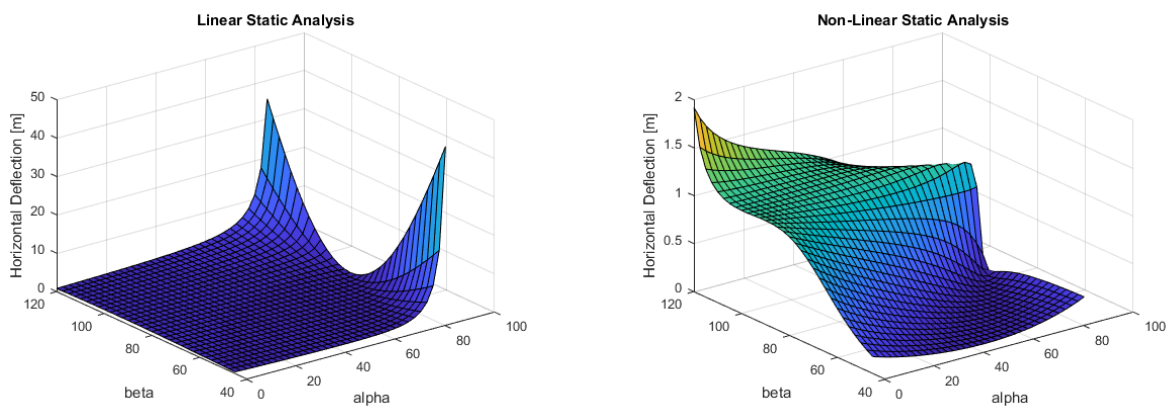
Figure 3.4: Static Horizontal Displacement for (a) linear and (b) non-linear spring forces, with respect to angles α and b

Discarding some of the unnecessary ranges and zooming into ranges α=0÷65 and β=0÷110 in both the linear and non-linear cases, similarities start becoming more evident, as in Figure 3.5.

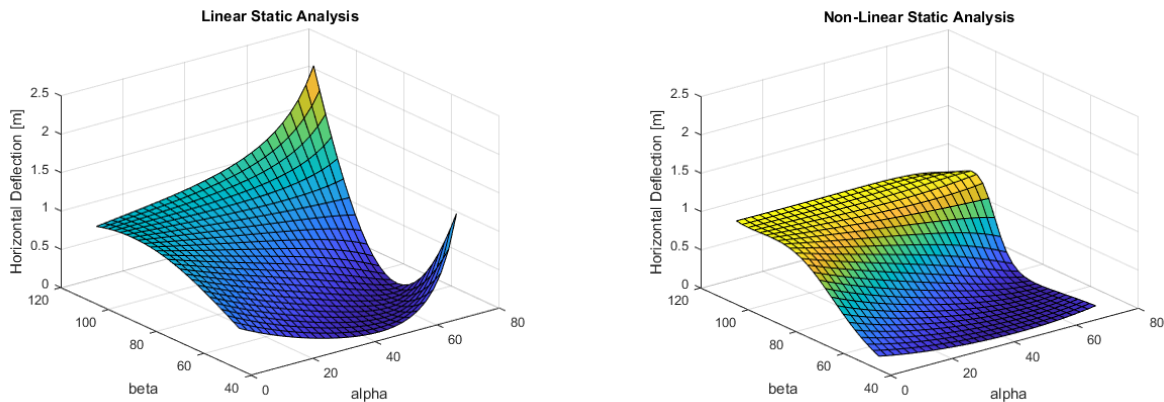**Figure 3.5: Static Horizontal Displacement for (a) linear and (b) non-linear spring forces, with respect to angles α and β**

In order to make the similarities even more evident, the two graphs are plotted into a logarithmic scale. An easy to observe pattern is formed for α=β, leading to the smallest horizontal deflections of the tunnel. This combination of angles leads to zero moments, as the spring forces pass through the cylinder centre, meaning that no rotation of the tunnel is caused. From the static problem, it has been seen that the rotational motion of the object amplifies the horizontal displacement of it[5]. Therefore, it can be concluded that the horizontal motions will reach a minimum for tethers aligned with the CoG of the tunnel, when no rotation takes place.
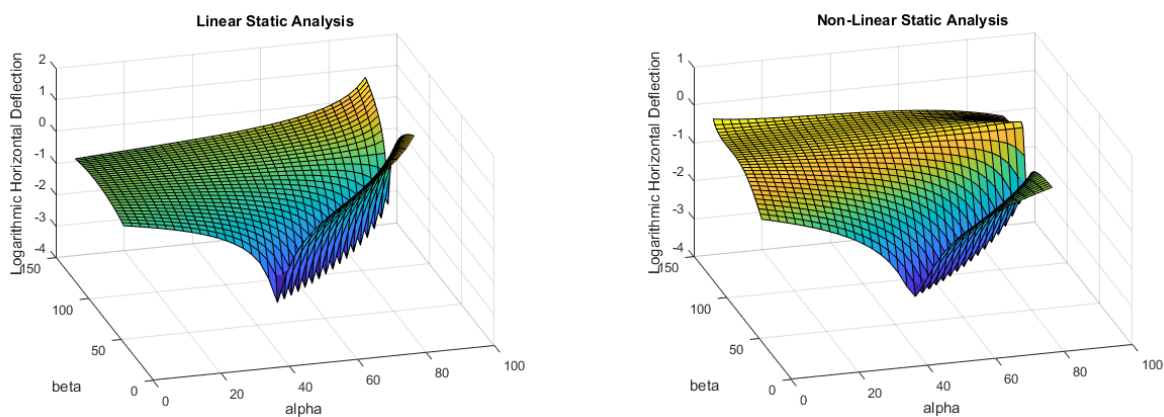

Figure 3.6: Static logarithmic horizontal displacement for a) linear and b) non-linear spring forces, wrt angles α and β

---

[5] Solving the static problem: $\begin{bmatrix} K_{xx} & K_{x\theta} \\ K_{\theta x} & K_{\theta\theta} \end{bmatrix} \begin{Bmatrix} u_x \\ u_\theta \end{Bmatrix} = \begin{bmatrix} F_x \\ 0 \end{bmatrix}$, one gets $u_x = \frac{F_x}{K_{xx} - \frac{K_{\theta x} K_{x\theta}}{K_{\theta\theta}}}$. When rotation is present, meaning a non zero value of $K_{\theta x} = K_{x\theta} \neq 0$, then the denominator becomes smaller and consequently u_x becomes larger. $K_{\theta\theta}$ is always a positive variable.
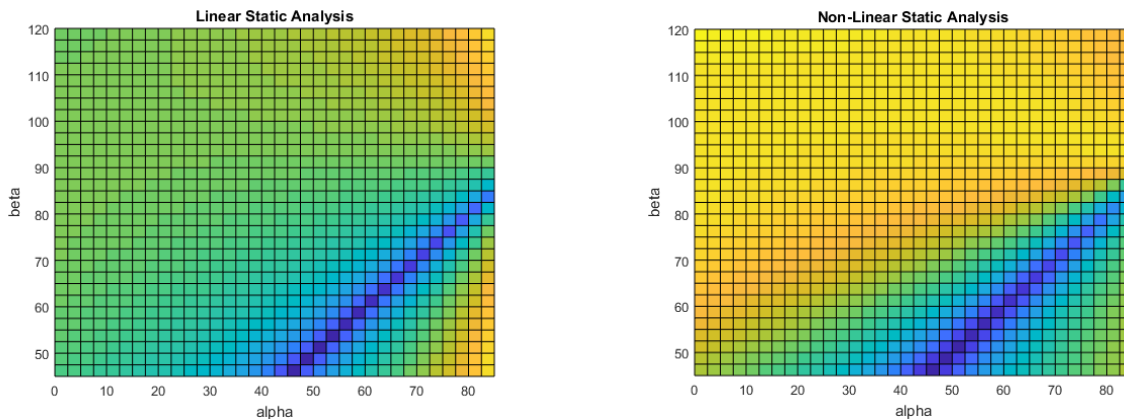
Figure 3.7: Top view of surface plots

3.4.2 β angles larger than 90º

Using an obtuse β angle to restrain the tunnel would be of great interest as it would allow the use of only one cemented foundation block at the seabed, as is depicted in Figure 3.8, reducing structural costs and making the SFT more appealing financially-wise.

Studying the surface plots of the tunnel's horizontal deflection, for both the linear and the non-linear cases, the model predicts some amplified motions, compared to other configurations. From Figure 3.5, these motions reach values to almost 1 m, which cannot be overlooked. This amplification can be justified by the increased lever distance of the axial tether force from the centre of the cylinder. Larger lever leads to larger moments caused by the tethers and consequently larger rotations. As it has been mentioned before, the rotational motion is coupled with the horizontal displacement of the tube.
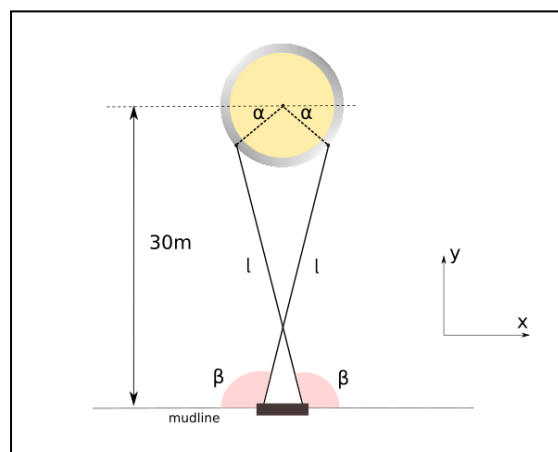

Figure 3.8: Tube restrained with one cemented foundation block

The analysis was limited to β angles up to 120º. If one increases the angle even further, reaching values up to 130º, the system becomes unstable. This was proven by running analyses with specific angle configurations, shown in Figure 3.9. The tunnel in black represents the initial position, while the blue shows how the tunnel is deformed after applying the static load. The tunnel is found to move backwards

in some cases, while totally flipping over in other, which is indicative of an unstable position. This behavior is the result of a negative tether stiffness, which is unreasonable.
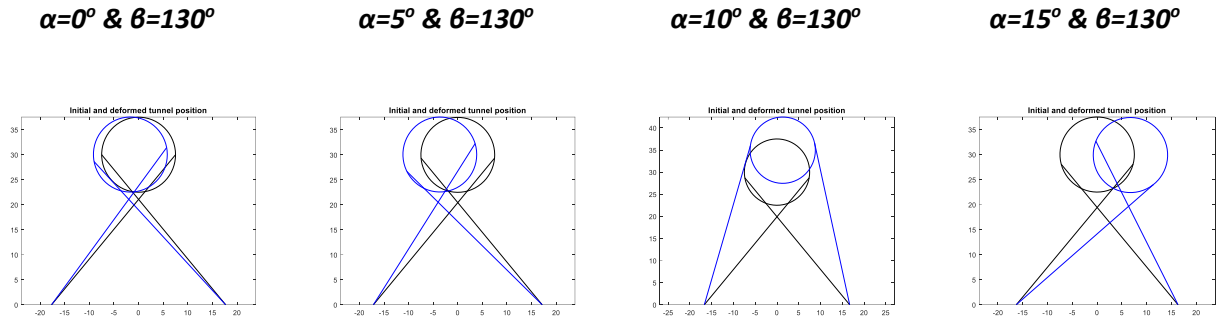
$\alpha=0^o$ & $\beta=130^o$ $\alpha=5^o$ & $\beta=130^o$ $\alpha=10^o$ & $\beta=130^o$ $\alpha=15^o$ & $\beta=130^o$

Figure 3.9: Initial (black) and Deformed (blue) position of the tunnel

3.5 Concluding to a tether configuration

Summarizing what was found from the 2D static analysis, a configuration with $\alpha = \beta$, with aligned tether angles, connection points and tunnel CoG provides the smallest horizontal displacements. Thus, it is desirable to use a configuration based on this criterion, further on, in the 3D modeling.

Unfortunately, there are some limiting factors that cannot be ignored. Installing the tethers under a small angle β ($< 45^o$) would provide quite a good horizontal stiffness, but it requires a lot of free space at the seabed for the foundation, which is not always available in narrow inlet areas like a fjord. In addition, the vertical motion of the tunnel needs to be taken care of.

Moreover, large angles α ($> 70^o$) are not wise to be used, from a structural point of view. The tunnel, due to its large volume, is exposed to large environmental loads. If the two tether connection points are close to each other, huge bending moments will be created at the area of the connection, that won't be possible to counteract. This will eventually lead to a structural failure. So it is suggested to connect the tethers as wide as possible.
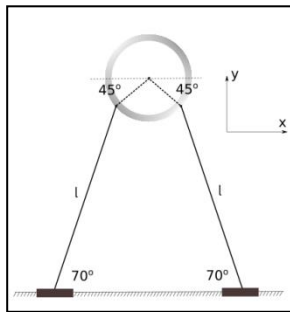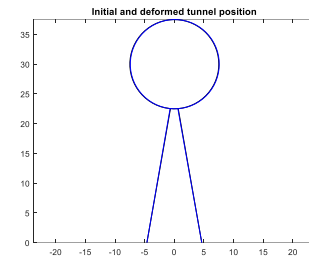
Reinertsen et al. (6) also performed some static analyses on their model and found approximate deflection values of $0.1 \div 0.2\ m$ for a comparable current loading. Taking everything into account, and trying to stay consistent with the prototype design, a configuration of $\alpha = 45^o$ and $\beta = 70^o$ was decided. It complies with all the limiting conditions and provides a solid support to the tube.

4 Tethers Spacing - 3D model

An optimum set of angles for the tunnel-tether configuration was identified, from the previous chapter, to be used further on. Another important parameter that defines how the tunnel responds to environmental loading is the number of tethers, and consequently the tunnel free span between two consecutive tethers. As the slenderness of the structure changes with changing number of tethers, the effect of vortex induced vibrations (VIV) can become extremely important, potentially damaging the structural integrity by reducing the fatigue life. The goal, of this chapter, is to predict how the amplitudes of oscillations in both the horizontal and the vertical direction change for a varying range of tethers used. Apart from checking whether the prototype design of 25 tethers is safe enough regarding VIV's, another question to answer is if a tether relief[6] could be possible.
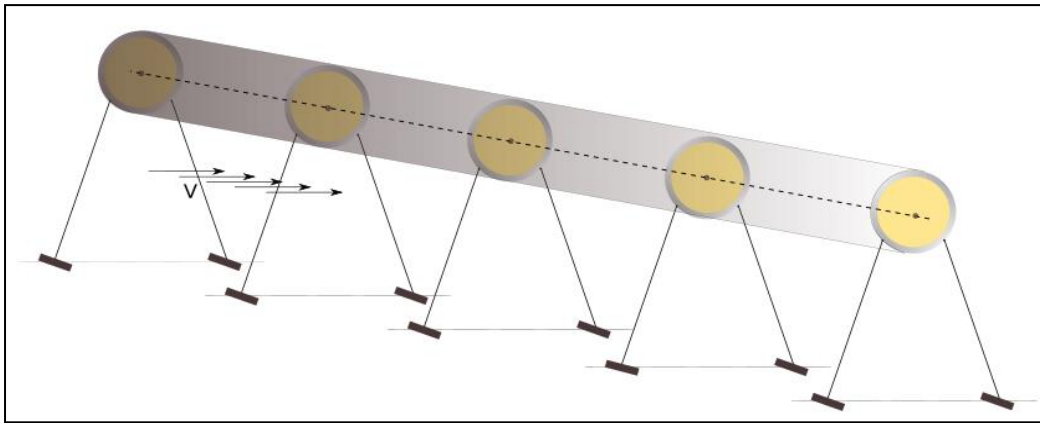

Figure 4.1: 3D tunnel overview

A 3D tunnel model has been developed to predict and quantify the significance of VIV's, based on the number of tethers used. The main challenge, here, lies on the coupling between the tunnel motions and the forcing terms coming from the current. As mentioned in chapter 2, the Van der Pol wake oscillator model has been used, a phenomenological model to predict VIV's. Vortex induced vibration experiments and theory focus mostly on short cylinders in two dimensional flows. An effort to predict the response of a large diameter structure has been conducted here. Due to lack of experimental data, similar values of the tuning parameters as for a low mass-damping system have been used[7]. This assumption will probably introduce deviations from the true tunnel deflection. Another assumption that is made, throughout the whole study, is that the vortex shedding behind the large diameter cylinder behaves similarly to a small diameter cylinder, and that it is capable to create significant vertical motions, to i.e. VIVs[8].

---

[6] Tether relief, meaning reducing the number of tether pairs used, without risking the integrity of the structure
[7] Tuning parameters: $\varepsilon = 0.7$ and $A = 12$
[8] This might not be fully true. If the motion is dominated by inertia forces, small frequencies of oscillation are to be expected, most probably, which means that small to none shedding will occur behind the cylinder. As there are not

An important aspect of the 3D model developed here that makes it stand out from other VIV models is that torsion is taken into account, while it is usually ignored when modeling other offshore, due to the significant difference in the diameter. While torsion doesn't affect the VIV phenomenon itself, it has large impact on the horizontal motion of the system. It would be a serious omission to ignore it, in the effort to capture the real tunnel displacements.

4.1   Tunnel modeling

The tunnel is modeled with Euler-Bernoulli beams, while the tethers have been replaced by linear springs with constant stiffness[9]. Each one of the 2nd order differential equations that describe the system, mentioned in chapter 2, are transformed into two 1st order equations. The explicit Runge-Kutta method is used to approximate the solution of the system iteratively, based on the previous step solution. The tunnel is discretized with N nodes, equally spaced along the tunnel length.

4.2   Eigenfrequency analysis

As a first step, the frequencies at which the system is prone to vibrate needs to be determined. The equation to be solved in order to estimate the eigenfrequencies and the eigenmodes of the structure is the undamped system's characteristic equation and is given by the expression:

$$|[K] - \omega^2[M]| = 0$$

The mass and stiffness matrices are assembled based on the finite element method, using beam elements with 5 DOFs, namely horizontal motion, vertical motion, tunnel longitudinal torsion, rotation around x-axis and rotation around y-axis. By using N nodes, the total number of DOFs is $5 \cdot N$. In addition to the material stiffness, some beam elements are affected also by the spring stiffness coming from the tethers. This additional component is added, based on chapter 3.3. The beam's element mass and stiffness matrix is shown below:

---

strong experimental data to support this statement, we assume that the shedding vortices are capable of creating significant vertical motions.

[9] As it was found in the 2D case, using either linear or non-linear springs gives similar responses, for the tether angles chosen. The similarities between linear and non-linear springs are also projected, for all the three tunnel motions, in Appendix A.

$$[K_{el}]=\begin{bmatrix} 12\dfrac{EI}{l^3} & 0 & 0 & -6\dfrac{EI}{l^2} & 0 & -12\dfrac{EI}{l^3} & 0 & 0 & -6\dfrac{EI}{l^2} & 0 \\[6pt] 0 & 12\dfrac{EI}{l^3} & 6\dfrac{EI}{l^2} & 0 & 0 & 0 & -12\dfrac{EI}{l^3} & 6\dfrac{EI}{l^2} & 0 & 0 \\[6pt] 0 & 6\dfrac{EI}{l^2} & 4\dfrac{EI}{l} & 0 & 0 & 0 & -6\dfrac{EI}{l^2} & 2\dfrac{EI}{l} & 0 & 0 \\[6pt] -6\dfrac{EI}{l^2} & 0 & 0 & 4\dfrac{EI}{l} & 0 & 6\dfrac{EI}{l^2} & 0 & 0 & 2\dfrac{EI}{l} & 0 \\[6pt] 0 & 0 & 0 & 0 & \dfrac{GT}{l} & 0 & 0 & 0 & 0 & -\dfrac{GT}{l} \\[6pt] -12\dfrac{EI}{l^3} & 0 & 0 & 6\dfrac{EI}{l^2} & 0 & 12\dfrac{EI}{l^3} & 0 & 0 & 6\dfrac{EI}{l^2} & 0 \\[6pt] 0 & -12\dfrac{EI}{l^3} & -6\dfrac{EI}{l^2} & 0 & 0 & 0 & 12\dfrac{EI}{l^3} & -6\dfrac{EI}{l^2} & 0 & 0 \\[6pt] 0 & 6\dfrac{EI}{l^2} & 2\dfrac{EI}{l} & 0 & 0 & 0 & -6\dfrac{EI}{l^2} & 4\dfrac{EI}{l} & 0 & 0 \\[6pt] -6\dfrac{EI}{l^2} & 0 & 0 & 2\dfrac{EI}{l} & 0 & 6\dfrac{EI}{l^2} & 0 & 0 & 4\dfrac{EI}{l} & 0 \\[6pt] 0 & 0 & 0 & 0 & -\dfrac{GT}{l} & 0 & 0 & 0 & 0 & \dfrac{GT}{l} \end{bmatrix}$$

$$[M_{el}]=\rho A\frac{l}{420}\begin{bmatrix} 156 & 0 & 0 & -22l & 0 & 54 & 0 & 0 & 13l & 0 \\[6pt] 0 & 156 & 22l & 0 & 0 & 0 & 54 & -13l & 0 & 0 \\[6pt] 0 & 22l & 4l^2 & 0 & 0 & 0 & 13l & -3l^2 & 0 & 0 \\[6pt] -22l & 0 & 0 & 4l^2 & 0 & -13l & 0 & 0 & -3l^2 & 0 \\[6pt] 0 & 0 & 0 & 0 & 140\dfrac{J}{A} & 0 & 0 & 0 & 0 & 70\dfrac{J}{A} \\[6pt] 54 & 0 & 0 & -13l & 0 & 156 & 0 & 0 & 22l & 0 \\[6pt] 0 & 54 & 13l & 0 & 0 & 0 & 156 & -22l & 0 & 0 \\[6pt] 0 & -13l & -3l^2 & 0 & 0 & 0 & -22l & 4l^2 & 0 & 0 \\[6pt] 13l & 0 & 0 & -3l^2 & 0 & 22l & 0 & 0 & 4l^2 & 0 \\[6pt] 0 & 0 & 0 & 0 & 70\dfrac{J}{A} & 0 & 0 & 0 & 0 & 140\dfrac{J}{A} \end{bmatrix}$$

4.3 VIV occurrence based on the number of tethers used

The response of the structure, subjected to current flow of *1m/s*, when the prototype design of 25 tethers is investigated, looks like in Figure 4.2. The 3D graph shows the deformed shape of the tunnel at

a random time, where steady state has been reached. Different axis scales have been used to make the deformations more visible. A top view and a front view are also included. An arc shape deformation is observed which is mainly caused by the constant drag force. Important to notice is that the middle points deflect the most throughout the total length of the tunnel. This will most probably cause the largest stresses on the middle tethers and will be analyzed later on.
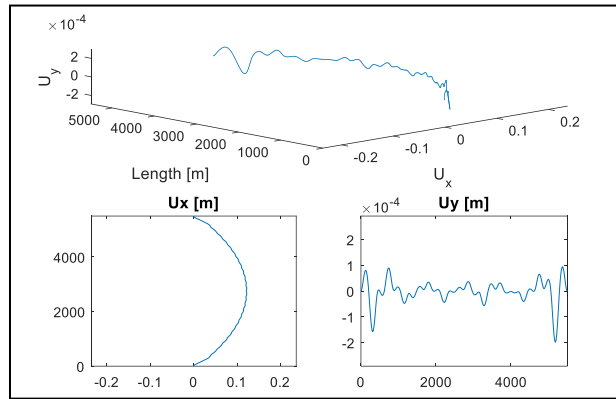
Figure 4.2: Simulation snapshot. a) 3D view of the tunnel's deformation b) top view c) front view

A mean of $\cong 0.12$ m deflection is observed horizontally with small vibrations in both directions, for a 5.5 km structure. This shows that the structure is quite stiff even when high current speeds occur. Figure 4.3 shows the motion of the tunnel center part, where the largest deflections are observed. While the current hits the structure, a new equilibrium position is reached, after countable oscillations. The in-line (blue curve) and the cross-flow oscillations are extremely small, almost negligible, when the steady state is reached.
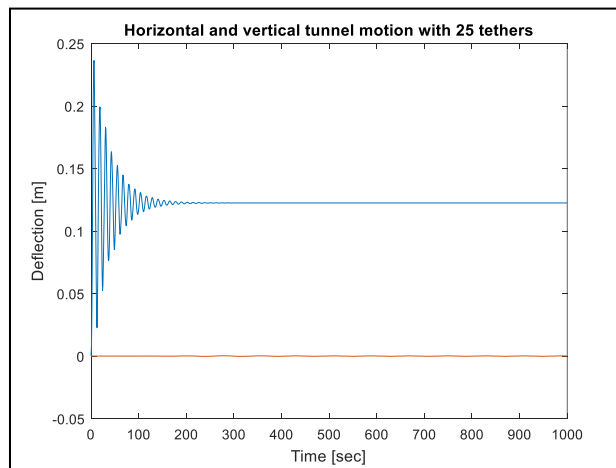
Figure 4.3: Horizontal (blue) and vertical (red) displacement of the tunnel point with the highest absolute deflection

This procedure is done for multiple tether configurations, starting from 25 tether pairs and dropping down to none. Figure 4.4 shows the maximum horizontal and vertical displacements, accordingly, for a current speed of 1m/s. In principle, the in-line motion of the tunnel is found to be larger than the cross-flow. This is something to be expected, taking into account the large constant drag that acts on the

cylinder. A sudden drop in the cross-flow direction line can be seen for a configuration of 15 tethers. Trying to interpret this behavior, this is probably caused either because the structure's natural frequencies are way far from the Strouhal frequency and, consequently, are not excited at all, or not enough modes have been used when modeling the structure and thus fail to capture the full motion of it. For a total number of 14 tethers, though, the displacements have already become significantly small, which wouldn't justify such a sudden drop to almost no motion.
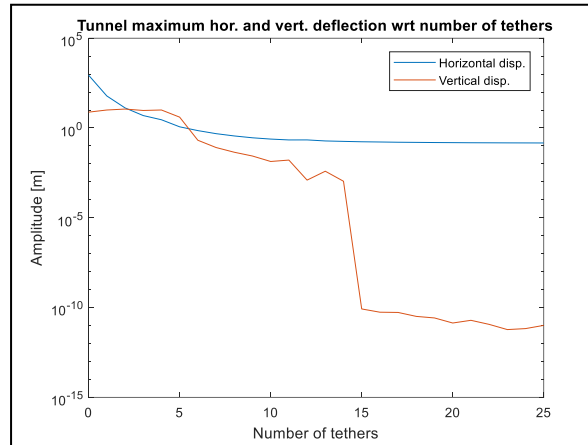

Figure 4.4: Maximum tunnel deflections wrt number of tethers

In Figure 4.5 the same exact response has been plotted, with indicative values projected. All the values shown are in meters. Design standards for such a structure, have not been developed yet, making it difficult to judge what is acceptable and what not. However, quantifying the tunnel's motion in the two directions, gives a good overview of what response to expect and design for.
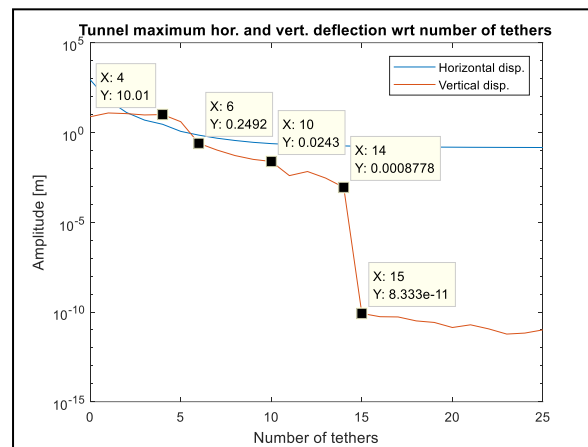

Figure 4.5: Indicative values of deflections

In order to reduce the computational time needed to approximate the solution of the system's motions while modeling the structure's motions, the modal superposition principle was implemented, initially using modes with frequencies $< 10 \cdot \omega_{st}$. This was chosen, because the area of interest was around the Strouhal frequency.

It became clear, though, that modes which are excited are not included and the model is not able to capture the proper tunnel motion, creating a numerical error. This justifies the sudden drop in the vertical oscillations, from Figure 4.4, where it was believed that after a certain tether number the vertical oscillations are diminishing to almost zero. Figure 4.6 shows the maximum tunnel in-line and cross-flow deflections using more modes, till frequencies $< 40 \cdot \omega_{st}$. Now the decrease in the response, while the number of tethers is increased, is much smoother, which is more reasonable.
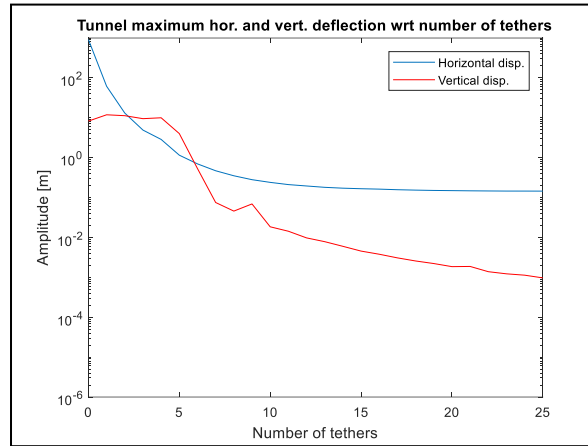

Figure 4.6: Maximum tunnel deflections wrt number of tethers (using more modes to reproduce the motion)

4.3.1   Dynamic drag component

In order to estimate the actual dynamic response of the structure, the mean drag component in the in-line direction needs to be removed. This is done by calculating and subtracting the mean from the total tunnel displacement, for a period of time when the steady state has been reached. This was observed to happen at around half the simulation cycles, where the simulation lasts 500 times the Strouhal period, approximately thirty minutes after the current hits the structure. Figure 4.7 shows the dynamic oscillations in both the directions. As it is expected, the cross-flow vortices are larger than the in-line.
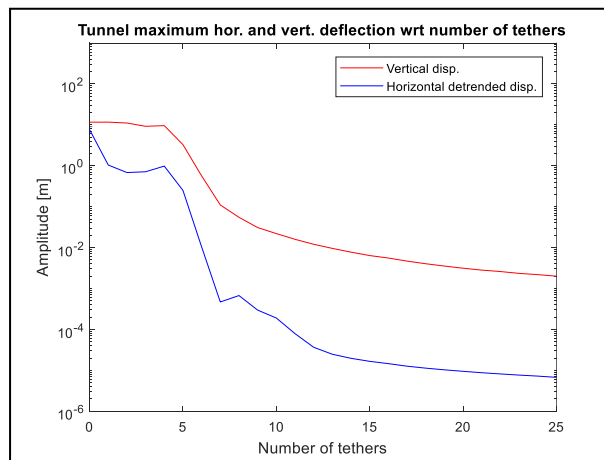

Figure 4.7: Maximum oscillation amplitude wrt number of tethers

Table 4.1 presents the amplitude values, coming from Figure 4.7. Only when a number of tethers around 7 is used, one could claim that VIV's start becoming of importance, with an oscillation amplitude of 7.5 cm. Vibrations of this magnitude can cause cracks and increase the fatigue damage of a concrete structure and therefore need to be treated carefully.

No. Teth	25	…	10	…	7	6	5	…	0
Vert. [m]	0.001		0.02		0.075	0.53	4		12
Hor. [m]	10^{-6}		$5 \cdot 10^{-5}$		$3 \cdot 10^{-4}$	0.0086	0.3		1

Table 4.1: Oscillation Amplitudes for cross-flow and in-line directions

4.3.2 Natural frequencies excited

When designing a structure it is always important to design it such that the range of its natural frequencies are far away from the frequency at which environmental forces are periodically applied, avoiding resonance phenomena. Therefore, it is of great necessity to check which modes are excited for each configuration and compare them with the Strouhal frequency. That said, in Figure 4.8, the first three modes with the highest contribution to the total nodal response, for each tether configuration, are plotted.
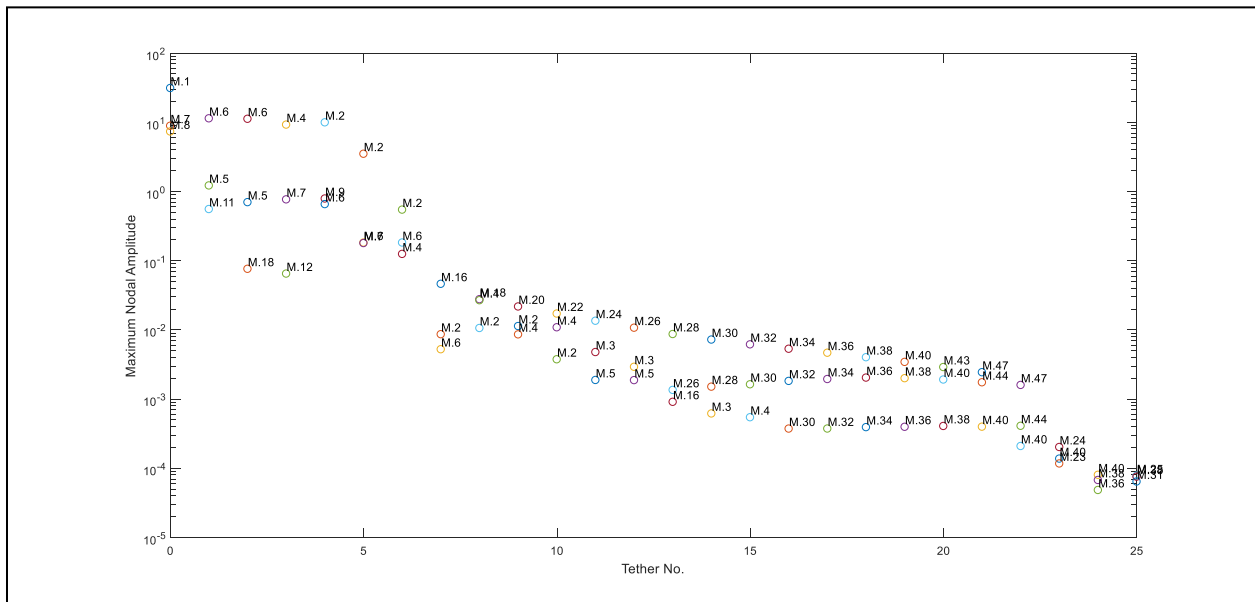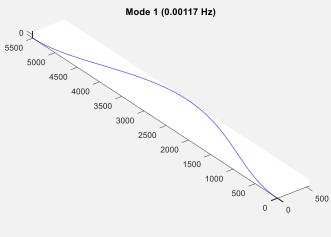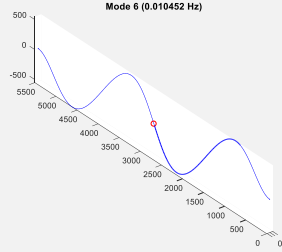

Figure 4.8: Natural frequencies excited per tether configuration

As modes coming from the vertical motion of the tunnel as well as the horizontal are mixed together, the graph doesn't give a proper overview of what each mode represents. Some modes are purely vertical, some purely horizontal and others are described by a combined motion.
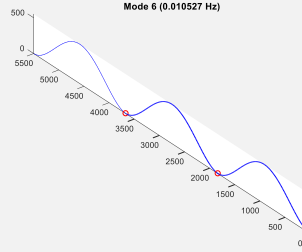
Table 4.2 shows the mode with the highest contribution, for each configuration, as well as its natural frequency. From previous chapters, the Strouhal frequency was found to be *0.013 Hz*.
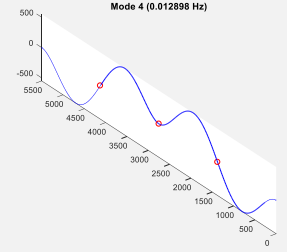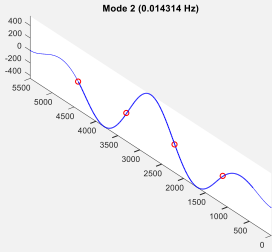
Mode 1 (0.00117 Hz)
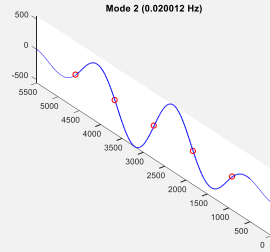
Mode 6 (0.010452 Hz)

Mode 6 (0.010527 Hz)

Mode 4 (0.012898 Hz)

No Tethers

1 Tether

2 Tethers

3 Tethers

Mode 2 (0.014314 Hz)

Mode 2 (0.020012 Hz)

Mode 2 (0.026733 Hz)

Mode 16 (0.074357 Hz)

4 Tethers

5 Tethers

6 Tethers

7 Tethers

Mode 18 (0.093815 Hz)

Mode 20 (0.11537 Hz)

Mode 22 (0.13893 Hz)

Mode 24 (0.16439 Hz)
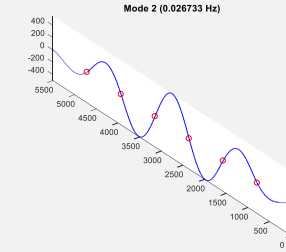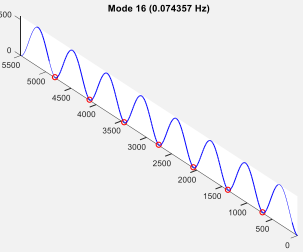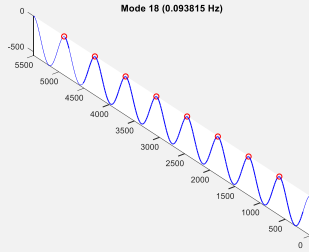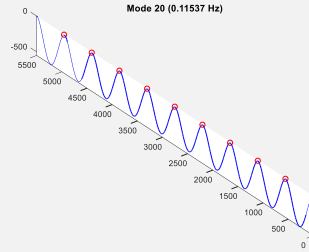
8 Tethers

9 Tethers

10 Tethers

11 Tethers

Mode 26 (0.19163 Hz)

Mode 28 (0.22051 Hz)

Mode 30 (0.25089 Hz)

Mode 32 (0.28262 Hz)
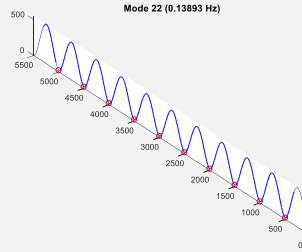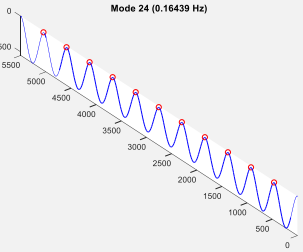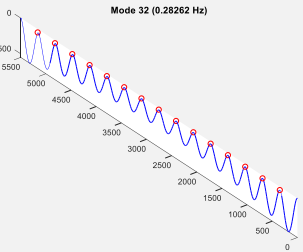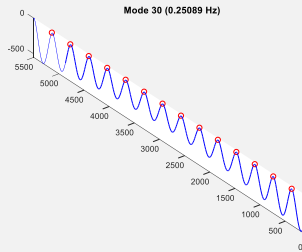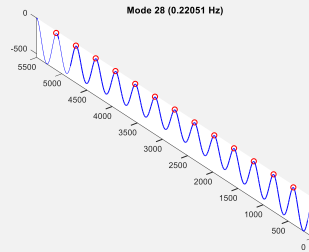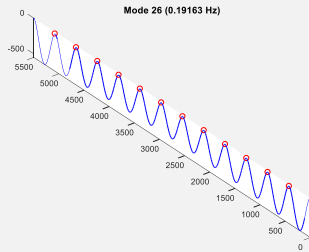
12 Tethers	13 Tethers	14 Tethers	15 Tethers
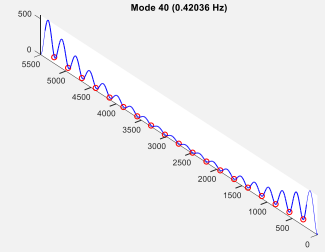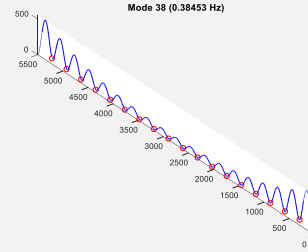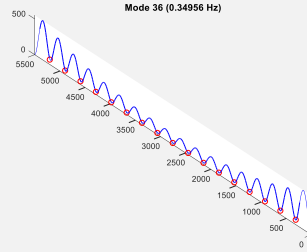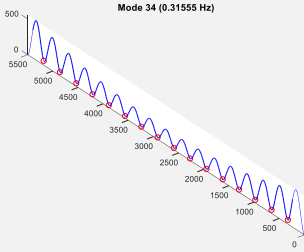
16 Tethers	17 Tethers	18 Tethers	19 Tethers
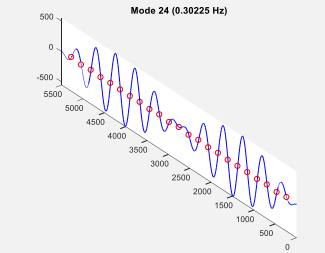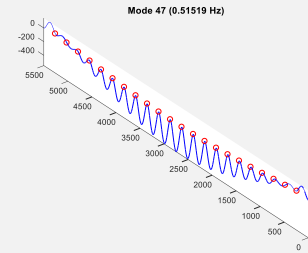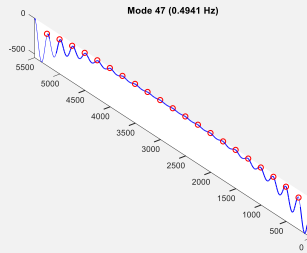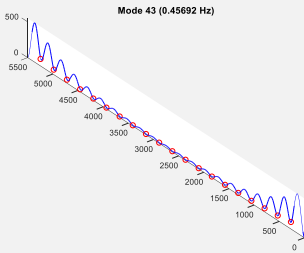
20 Tethers	21 Tethers	22 Tethers	23 Tethers
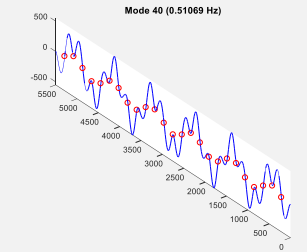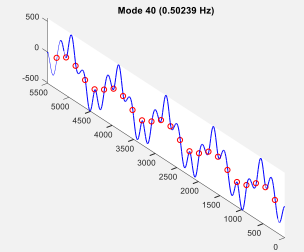
24 Tethers	25 Tethers

Table 4.2: Modes contributing the most to the tunnel motion, per configuration

4.3.3   Stresses on tethers

Till now, focus has been put on the deflection of the tube. An important aspect of the design, though, is the tether stress capacity. Tethers are designed such that can withstand the loads and restrain the tunnel motions, without failing. For this, the axial stress on each tether needs to be found. In order to

calculate the axial stress on the tethers and evaluate the structural integrity of each number of tether's configuration, the tension created by the motion of the tunnel is calculated.

The tethers positioned in the middle of the tunnel are the one experiencing the largest stresses, due to the largest deflections at this region. This is something easily observed from the deformed shape of the tunnel on Figure 4.2. Moreover, the upstream tether is considered the critical one, carrying the largest load. Therefore, it makes sense to focus on the stress of the middle tether, as the one experiencing the highest stresses. In order to find the stresses, first, the tension is found by multiplying the tether deformation with its axial stiffness:

$$\Delta N = \overline{u_T} \cdot \frac{EA}{l}$$

where, EA is the axial stiffness of the tether and l is the length of the tether. The elongation of the tether is extracted from the simulation, accordingly, taking into account the translational motion of the tunnel, as well as the rotational motion of the connection point between tether and tunnel.

In the offshore industry an undesirable phenomenon when dealing with tensioned mooring systems is the slacking of the tethers. In order to avoid such phenomena it is important to install the tethers under a constant pre-tension. The needed nominal pre-tension per tether is ≈10MN (Reinertsen et all., 2016b). Summing up the constant pre-tension and the varying part and dividing by the cross-sectional area of the tether, the axial stresses are found, as depicted in Figure 4.9. The dashed red line, depicted, represents the yielding strength of the S235 steel, above which, plastic deformations occur. It can be seen that the minimum number that can withstand the static and the dynamic environmental loading, without taking into account any safety factor, is the configuration of 10 tethers.
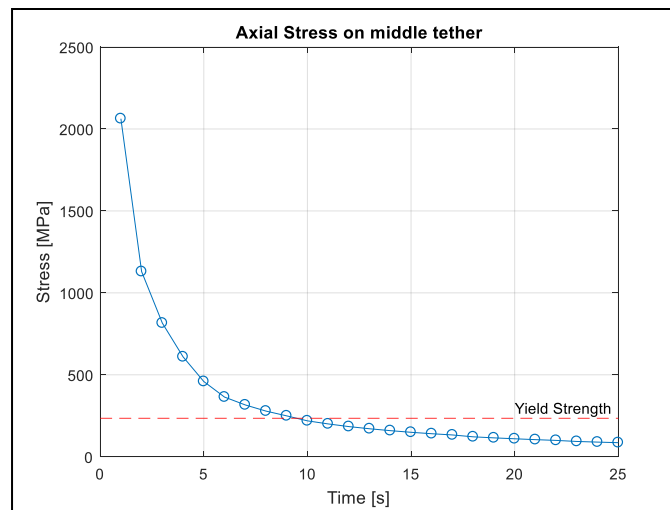
Figure 4.9: Middle tether stress per configuration

An assumption made early on, in order to calculate the tether stiffness using the linear spring approach, is that the tension has to remain pretty much constant. Based on the 10MN pre-tension, as well as the known cross sectional area of the tethers, a pre-stress of 100MPa is found, approximately. From Figure

4.9, a stress close to this value is obtained for a number of tethers above 20. The rest are violating this assumption, which will probably introduce some small errors. A more accurate approach would be to estimate the tether stiffness using non-linear springs, which allows a varying tether tension.

4.3.4   Impact of waves on the tunnel

Till now, we analyzed the effect of current loading on the SFT. In this chapter, the effect of the wave loading will be examined, in comparison to the current. From the wave conditions present at the Bjornefjord offshore location (Petterson, 2007), a wave period of 14 s for swell and 4.5 s for wind-sea waves is used as the 100 year sea state. The exponential decay of the waves is visualized in Figure 4.10, where it can be seen that the swell waves are the most dominant loading factor, at a reference depth of -30m. Wind generated waves reach significantly large amplitudes at the sea surface, but decrease rapidly to an inconsiderable wave amplitude at -30 m water depth.
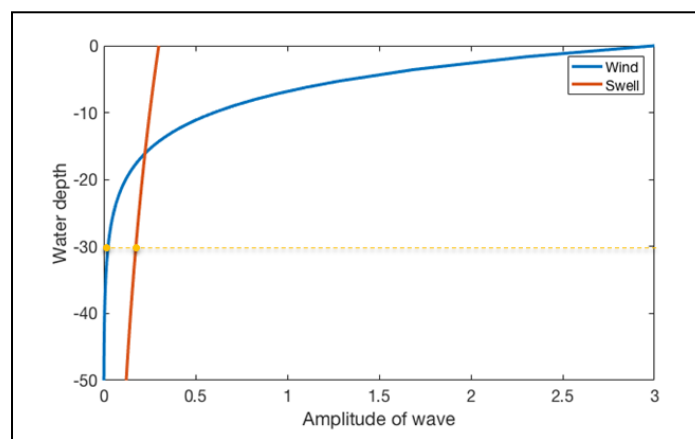
Figure 4.10: Wind-sea and swell wave profile

In order to estimate the wave forces acting on the tunnel, the principles of the Airy wave theory are applied. Eckhart's approximation gives a good estimation of the wave number and, consequently, the wave length. For swell, a wave length of 310 m is found. Based on Table 4.3, and given that $h/\lambda = 60/310 = 0.19$, intermediate water depths are assumed on site, where both the water depth and the wavelength have a significant influence on the solution of the theory.

Properties of gravity waves on the surface of deep water, shallow water and intermediate water depths, according to Airy wave theory				
Quantity	**units**	**deep water (h>0.5λ)**	**shallow water (h<0.05λ)**	**intermediate depth (everything else)**
Wave phase	$\theta(x,t)$	$kx - \omega t$		
Dispersion relation	rad/s	$\omega(k) = \sqrt{gk}$	$\omega(k) = k\sqrt{gh}$	$\omega(k) = \sqrt{gktanh(kh)}$
pressure oscillation	N/m^2	$\rho g\alpha e^{kz}cos\theta$	$\rho g\alpha cos\theta$	$\rho g\alpha \dfrac{cosh\big(k(z+h)\big)}{cosh(kh)}cos\theta$

Table 4.3: Wave properties from the Airy wave theory

Wave forces are split into two large categories, viscous forces and inertial forces. Viscous forces are mostly related to the flow separation behind the cylinder, whereas inertial forces arise from the potential flow wave theory with components like the Froude-Krylov and diffraction forces. The Keulegan-Carpenter number describes the relative importance of the viscous forces over the inertial forces on an oscillatory flow. It is given by the relation:

$$K_c = \frac{V \cdot T}{D} = \frac{\lambda}{D} \cong 0.15$$

From theory, for $K_c < 1$ no appreciable flow separation takes place, meaning that it is valid to ignore the viscous/drag forces. This said, in order to estimate the wave forces on the tube, only the inertial forces need to be calculated.

The Froude-Krylov force or incident wave force is found by integrating the water pressure around the circumference of the tube. To do this, the cylinder has been discretized into multiple points, like in Figure 4.11, and the force components in each point is calculated based on expressions:

$$dF_{x,i} = p(x,y,t) \cdot ds \cdot cos\varphi$$

$$dF_{y,i} = p(x,y,t) \cdot ds \cdot sin\varphi$$

Summing up all the components one can reform the resultant *FK*-force.
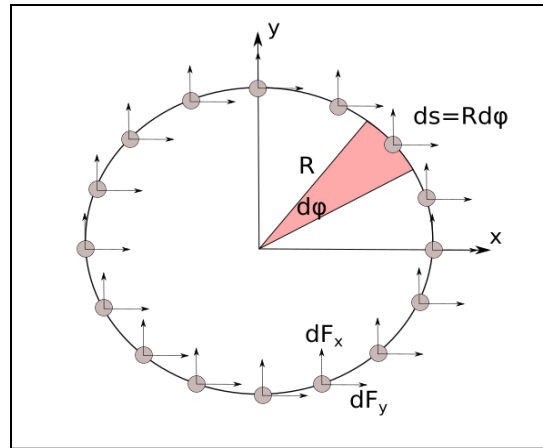
Figure 4.11: Pressure integration along the cylinder circumference

Figure 4.12.a projects the magnitude of the wave force (red) in comparison to the current force (blue). The magnitude of the *FK*-force is approximately half the one created by the current. It has been found that the current force cannot produce significant displacements in tether configurations with multiple tethers used, like the prototype design. The same cannot be concluded for the wave force though, despite the smaller amplitude. The reason is that the wave frequency is way higher than the current oscillation frequency and close to the first natural frequency of the system. Consequently, resonant phenomena can arise from the application of the wave force with larger impact on the structure than what is predicted for the current. Figure 4.12.b shows the direction of each force. While the current force only directs towards the flow direction, due to the mean drag force, and fluctuates around 0° due to the lift forces, the wave resultant force rotates around the cylinder, which can be understood by the sudden jump from the 180° angle to -180° and rises again.
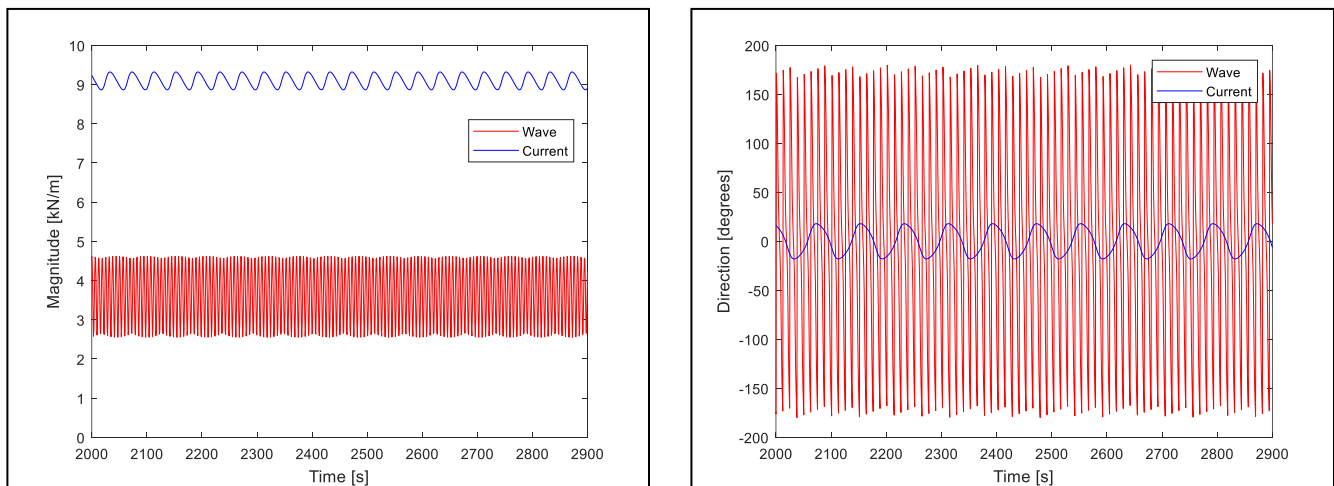
Figure 4.12.a: Magnitude of the resultant force created by waves and current, b. Direction of the resultant force created by waves and current

From the wave force estimation it can be concluded that while the magnitude is of the same order as the one coming from a current flow, the impact each force has on the structure is totally different, due

to the difference in the excitation frequencies. As a result, a more analytical calculation of the wave force needs to be performed including the diffraction part, in order to evaluate the complete effect on the SFT.

5 Structural failure of a tether

5.1 Introduction

Till now, the robustness of the structure, regarding the environmental conditions during operation phase, has been proven. The configurations that can withstand the combined action of static and dynamic loads have been defined. In this chapter, the unexpected loss of one tether is investigated. The goal is to evaluate the overall safety of the tunnel tube when a tether fails by checking if the energy released from the failed pre-tensioned tether is capable of causing a consequent damage to more tethers, or if the structure finds a new equilibrium position safely, without putting human lives in danger.

For this, an unexpected failure on the middle tether pair, half way through the length of the tunnel, will be applied. As the tunnel is restrained with two tethers per tether point, one upstream and another downstream, the effect of one of the two failing as well as both failing will be examined.

5.2 Tether failure on the prototype design

The failure is applied at the system, at time t, after the steady state has been reached and the tunnel moves only due to the current flow. At that time, the tether stiffness is removed and the tunnel is left to find a new equilibrium position. Stresses on the other tethers are constantly monitored and when the stress capacity is reached, another failure is introduced.

In Figure 5.1, a snapshot of the analysis is shown. Each active upstream tether is represented by a green circle and each active downstream tether by a green cross. When a tether fails, instantly becomes red, as is shown for the left middle tether. Subplot on top left shows the 3D representation of the tunnel motion, the top right subplot shows the vertical motion, the bottom right the horizontal motion and the bottom left gives a view from the side. All the units are in meters, meaning that when the tether is failing, the tunnel is locally deformed, reaching a deflection of ≈0.4 m.

The snapshot is taken at a time when a new equilibrium has almost been reached. This means that no further failure is observed.
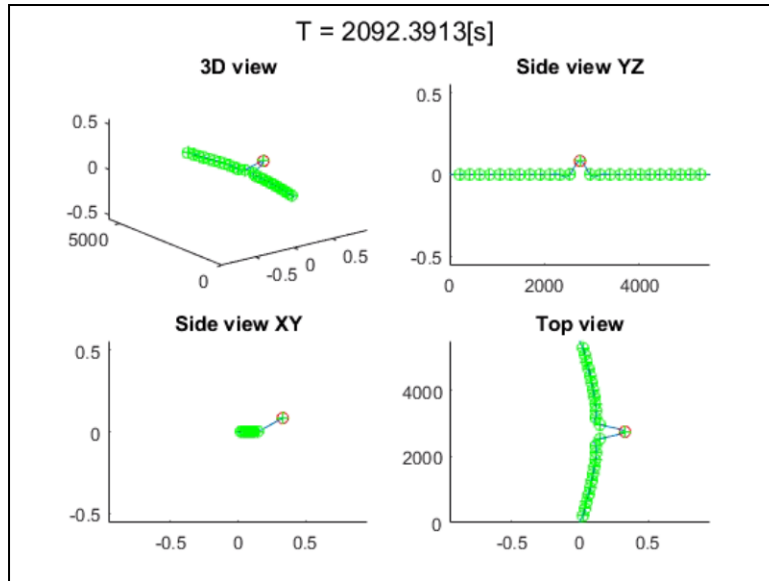
Figure 5.1: Snapshot of left middle tether failing

In the case of both the upstream and downstream tethers failing, Figure 5.2, the deformation of the tunnel is smaller in the horizontal direction. The vertical motion, though, is amplified. This happens because a larger tunnel segment is exposed, unrestrained. The larger buoyant forces stretch the tunnel upwards, leading to reduced in-flow motion.

Again, no progressive structural failure is observed that can threaten the integrity of the complete structure. Consequently, the prototype design is quite robust when a tether or a pair of tethers fail, providing the necessary time for the replacement of the damage. It is also safe to state that VIV's won't be a problem for the new free span section of 400 m, as it has been found that a free span of ≈700 m is needed for the amplitudes of oscillations to reach significant values.
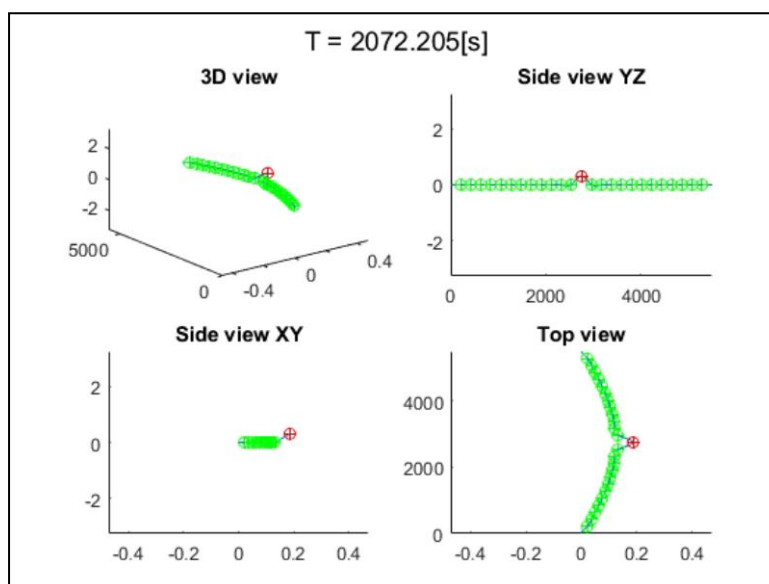
5.3   Tether failure on relaxed tether configurations

Now that the safety of the prototype design has been proven, regarding current loading, the question that arises is if the structure has been overdesigned to withstand all these failure uncertainties and if there is margin for a tether relaxation without putting the structural integrity at risk.

In order to do so, based on the axial tether stresses, the 'limiting case' configuration that can withstand the static and dynamic loads needs to be defined. Similar procedure to the one in §4.2.4 is followed, with the only difference being the safety factors introduced. A value of 1.2 is used for the steel strength, resulting in a 27 MN tether capacity.

Figure 5.3 shows the 14 tether configuration exactly before the left middle tether fails. The structure is loaded by a current flow, and is still able to withstand both the static and the dynamic loading. Figure 5.4 depicts when the tether failure occurs, while Figure 5.5 shows the system equilibrium position after the structural failure has been applied and a sufficient amount of time has passed for a steady state condition to be reached. It can be observed that the remaining tethers are not able to carry the load and have progressively failed.
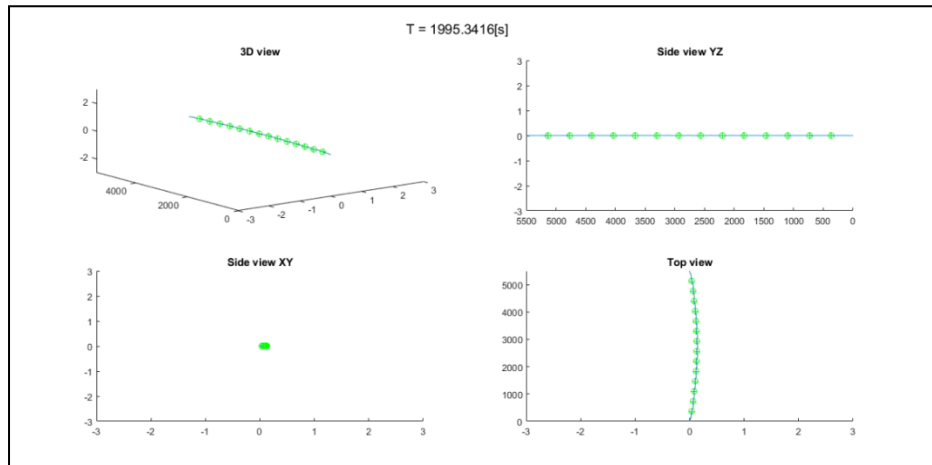
Figure 5.3: Before tether failure, 14 tethers configuration
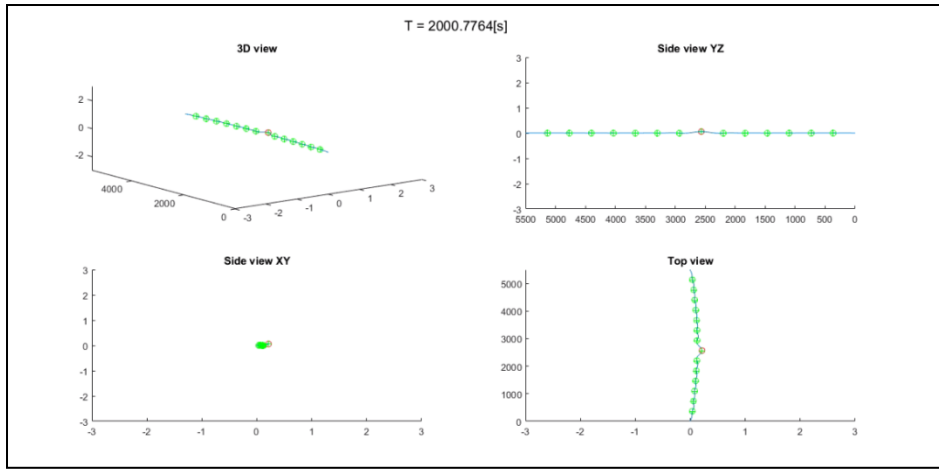
Figure 5.4: Exactly after left tether failure, 14 tether configuration
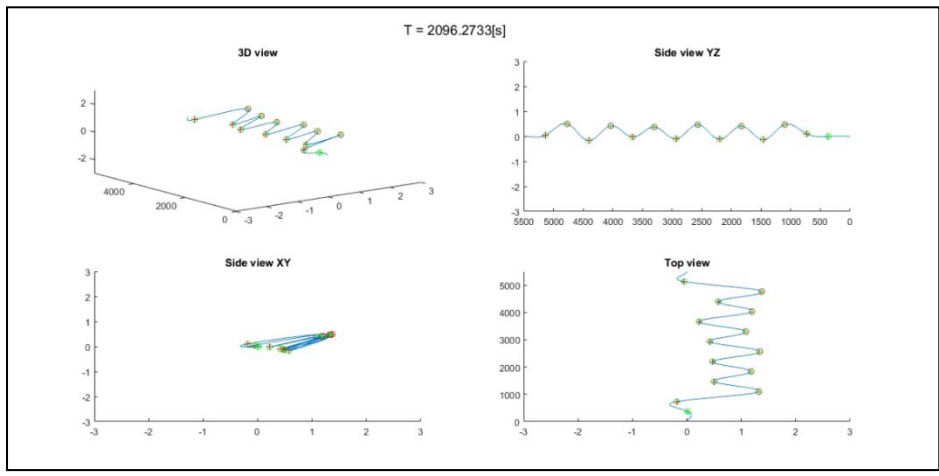
Figure 5.5: Almost two minutes after tether failure, 14 tethers configuration

Having defined the response on the prototype design (25 tethers), as well as the 'limiting case' configuration (14 tethers), all the in between configurations will be analyzed. The goal, once more, is to define for which number of tethers, the structure can resist consecutive damage when one tether failure occurs.

Table 5.1 summarizes the results from all the simulations run, with '✘' meaning that more tether failures occur when one tether fails, and '✓' meaning no consecutive tether failure. It becomes clear that only the 24 and 25 tether configurations are resistant in all possible failure cases. Based on the used environmental conditions, as well as the safety factors[10], the 25 tether configuration is considered ideal and no further constraint relief is advisable.

---

[10] It is reminded that a material safety factor has been used, based on pure engineering judgment. It is not based on official offshore standards and regulations, as these do not exist for such a structure.

No. Tethers		14	15	16	17	18	19	20	21	22	23	24	25
Chain reaction failure non-sensitive	Middle left tether fails	✗	✗	✗	✗	✗	✗	✗	✗	✗	✗	✓	✓
	Middle right tether fails	✗	✓	✓	✓	✓	✓	✓	✓	✓	✓	✓	✓
	Both middle tethers fail	✗	✗	✓	✓	✓	✓	✓	✓	✓	✓	✓	✓

Table 5.1: Configurations non-sensitive to progressive failure

It is important to mention that, while the failure was applied in the middle section of the tunnel, more starting points were examined, all with smaller impact than the one starting from the middle tether pair.

6 Installation plan

This chapter gives a brief overview of the Bjornefjord SFT installation plan, the assumptions, the methods and tools/vessels used for the major marine operations, based on Olav Olsen's feasibility report (6). In principle, multiple techniques and experiences from the offshore industry have been applied in the development of this challenging bridge concept.

The complete installation of the SFT requires complex marine operations, controlling the 5.5km tunnel string, as well as detailed planning of all the project stages in order to minimize the execution risk. A large number of towing vessels and personnel have to be mobilized for all these procedures. This makes the whole process extremely challenging. Adding up to the complexity of the operations, all the major operations need to be performed within certain weather windows. The major marine installation items for the tether stabilized SFT are:

- Rock tunnel plugs
- Landfalls/foundation caissons
- SFT elements
- Rock anchor piles
- Tethers
- Temporary buoyancy shafts
- Solid ballast SFT end boxes
- Solid ballast landfalls

6.1 Building operations

6.1.1 Temporary mooring system and SFT assembly

The assembly of the SFT elements will be performed afloat, in a sheltered fjord, close to the installation location in the Bjornefjord site to avoid wave and current excitations, as seen in Figure 6.1. The location is suitable given the final geometry of the tube and provides the necessary space for vessel access and maneuvering, while the towing distance is small compared to other alternatives.

Figure 6.1: Bjornefjord site and sheltered location

The temporary mooring system includes offshore mooring lines connected to tension barges and onshore bollard posts, as shown in Figure 6.2. This supporting configuration is planned to be used also for the joining operations.
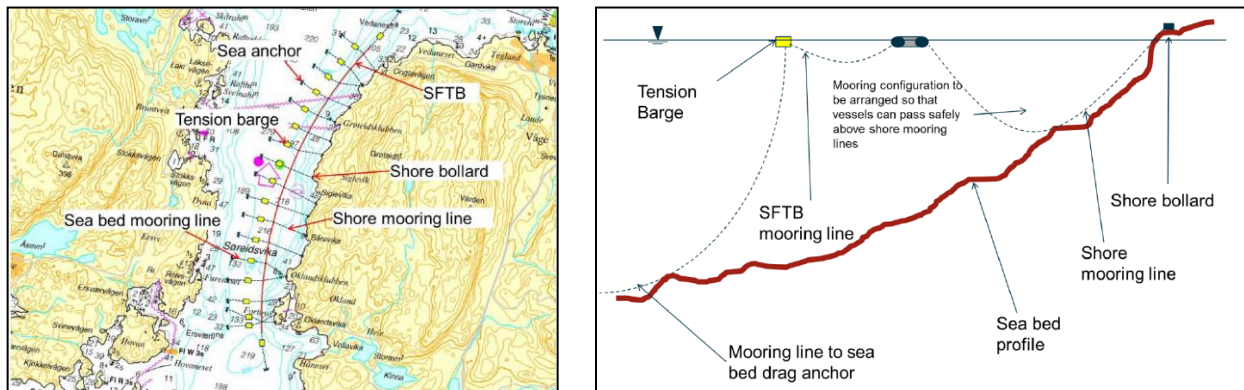
Figure 6.2: Temporary mooring system

When a new tunnel element is in place to be connected with the main body of the SFT, the steps below are followed:

1. Adjust guides and shims to cater for tolerances
2. Moor new section
3. Adjust trim with ballast
4. Winch elements against guide system
5. Secure elements first with winches and then with bolts
6. Install cofferdam and discharge water
7. Install scaffolding and perform concrete welding first on tube and then internally
8. Perform pre-stressing
9. Perform pressure testing
10. Remove cofferdam

6.1.2   Installation of rock plugs and landfalls

Prior to the installation of the rock plugs the seafloor is straightened and guides are placed. A pull-in winch will be used to position the element when it is on top of the guides. An ROV will monitor the positions and connect the wire. While in target position, additional water ballast is provided and the temporary buoyancy shafts, used to sink the element, are ready to be removed.
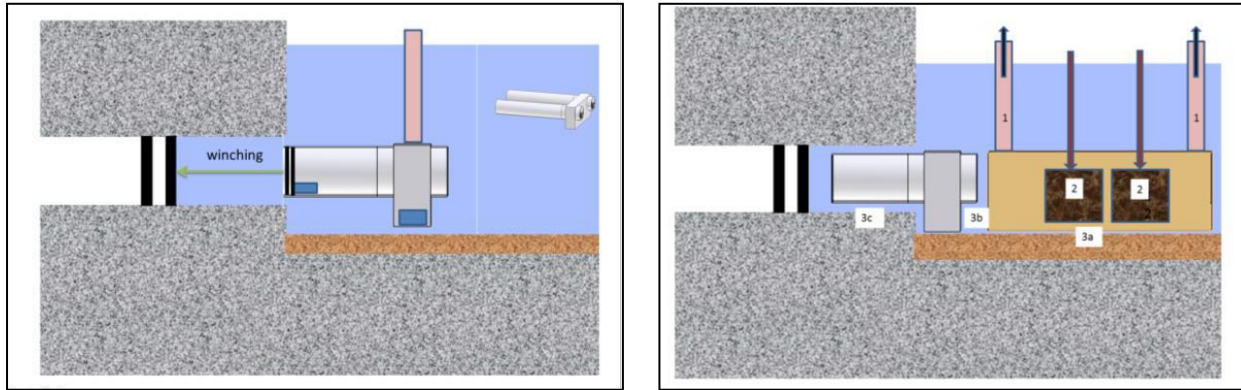
6.3: **North and south rock plugs and landfalls**

The installation of the landfalls is similar to the one for the rock plugs. When the landfalls are in position the procedure continues as follows:
1. Remove temporary buoyancy shafts
2. Fill with iron ore (solid ballast) using rock filling vessels
3. Connect with the rock plugs

6.1.3   Installation of rock anchors

The soil is suitable for the use of rock anchors. The main operational steps for the preparation of the anchor foundations are:
1. Drill casing and drill bedrock
2. Grout casing
3. Drill through casing and 40m into bedrock
4. Position rock anchor pile into hole
5. Grout the pile with the casing
6. Perform load testing with a design load of 20MN (10MN pre-tension on each tether is designed)

6.1.4   Installation of tethers

The tethers will start being installed approximately 1,5 years prior to the SFT installation date. The plan is to tow the tethers horizontally and upend them, as was performed with the Heidrun TLP tethers. Tug boats with bollard pull of 40-50 t will be mobilized. A trailing tub will also be used, responsible for the lowering of the bottom tether part with a winch, during upending. The top part of the tether will be supported by an offshore construction vessel with an offshore crane included on board.
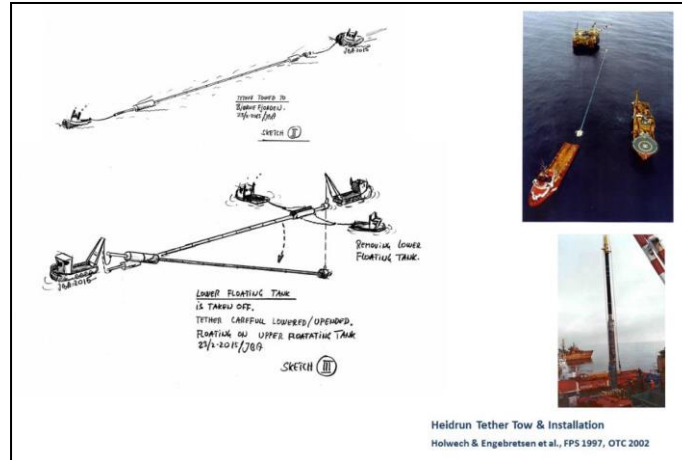
Figure 6.4: Tether transport and upending

Each pair of tethers is planned to be tied together, in order to avoid VIV's or other phenomena. A hold back system, comprising of an anchor and a clump weight, will be used to prevent any contact during the SFT submergence.

6.2   SFT tow and landfall hook-up

Towing of the entire SFT requires extensive planning and preparations. Lots of parameters need to be accounted for a safe execution. Some crucial variables to be considered is the towing resistance of the points from which the towing will take place, the route which will be followed, the number of tug boats required to pull the complete structure, as well as the stiffness on the mooring lines. To be fully aware of all the aspects, scale model tests are included, extensive inspections of the structural parts and simulation trainings of the personnel in charge will take place.

In principle the SFT optimally will be towed sideways. This way the bending of the tunnel, caused by surface waves, is minimized during the transportation. Only when the SFT starts from the sheltered fjord, tug boats from one end will pull the tunnel string in-line, due to the limited width span present. The tug boats need to be able to overcome the created drag force, created by the interaction of the structure with the fluid. Assuming a drag coefficient of 2, a quick estimation of the drag force is found based on a current speed of $0.3\,m/s$:

$$F_D = \frac{1}{2}\rho C_d DLV^2 \cong 7425 kN$$

Assuming an efficiency of 0.7 on the tug boats, the thrust requirement is $10607 kN$ or $1082 t$. This means that approximately 10 tug boats are required per direction with a towing capacity of 100-150 tones each.
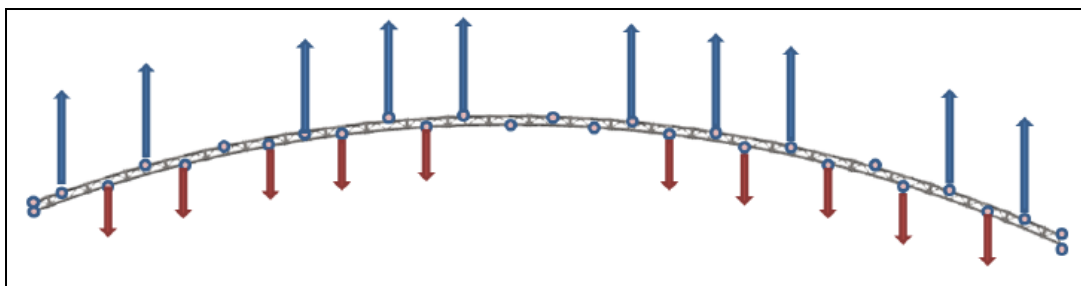
Further investigation on cross-flow VIV's is required during the temporary phase of SFT transportation, when it is not fully supported. VIV's can make their present in two critical moments during the whole operation. While the towing is performed at the sea surface and during the submergence operation. The way to control VIV's is by changing the stiffness of the structure. This is done by adding extra water weight inside the buoyancy shafts installed on top of the SFT, responsible for the submergence as it will be explained later on.
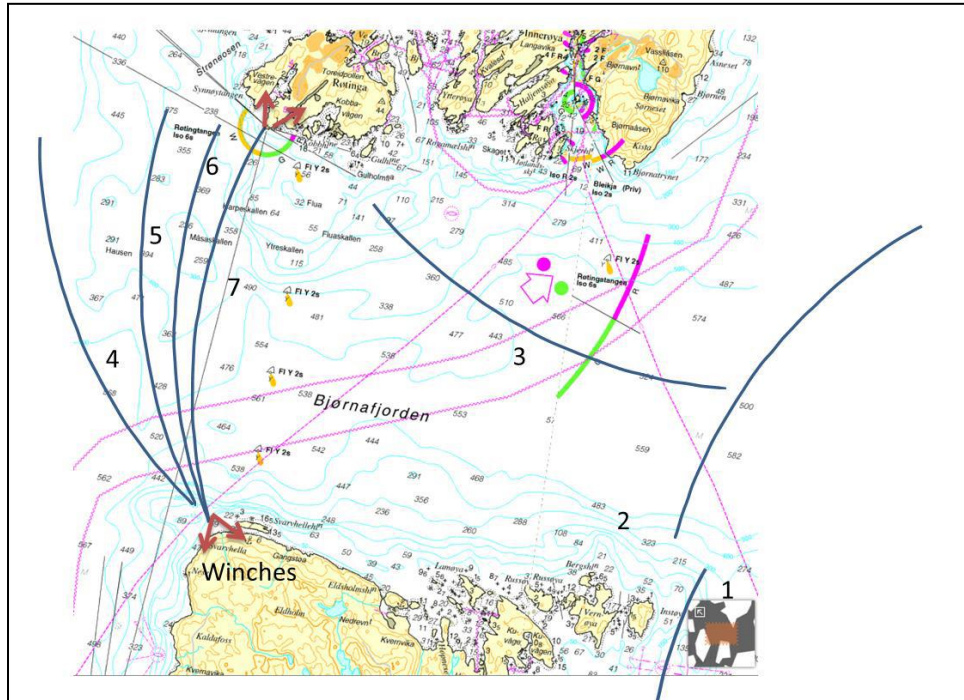
Figure 6.6: Transportation plan

Figure 6.6 shows the maneuvering of the SFT till the final position. When the tunnel is at the desired location the two ends are connected to shore winches. Till the SFT is successfully connected to the landfalls, the tug boats remain active. As soon as the shore winches are connected, the ballasting can take place.
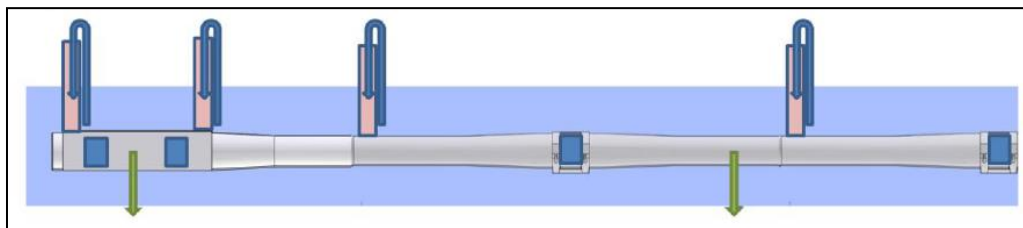
Figure 6.7: Buoyancy shafts for the SFT submergence

Multiple temporary buoyancy shafts will be used to manage the submergence of the SFT. Each shaft includes pumps to add water, as well as de-ballasting pumps to reverse the operation at any point needed. The tug boats remain in a supporting arrangement. At the last stage of the ballasting, the SFT end positions will be adjusted by the winches and pulled tight against the guides on the landfalls.

Having secured the connection on the two ends, based on calculations performed by Olav Olsen group, the remaining operations are not directly time critical, as the only constraint is to connect the tethers before fall season. The tugs can be demobilized, and the configuration has been documented to withstand the 10 year return period storm.

6.3 Tether hook-up

The last part of the installation procedure is connecting the tethers to the main tube. The buoyancy shafts are still active, providing stability.

Prior to operation, the top connector assemblies for the tethers are pre-rigged over the tether porches and the locking gate in each porch is open, as shown in Figure 6.8. Each tether is guided inside the corresponding porch by ROVs and the gate is closed. This is done for all tethers, while none is loaded. The top connectors lock the tethers hydraulically and the tube segment is de-ballasted to apply the pre-tension. This procedure is done in a controlled sequence, each time monitoring the tunnel displacements.
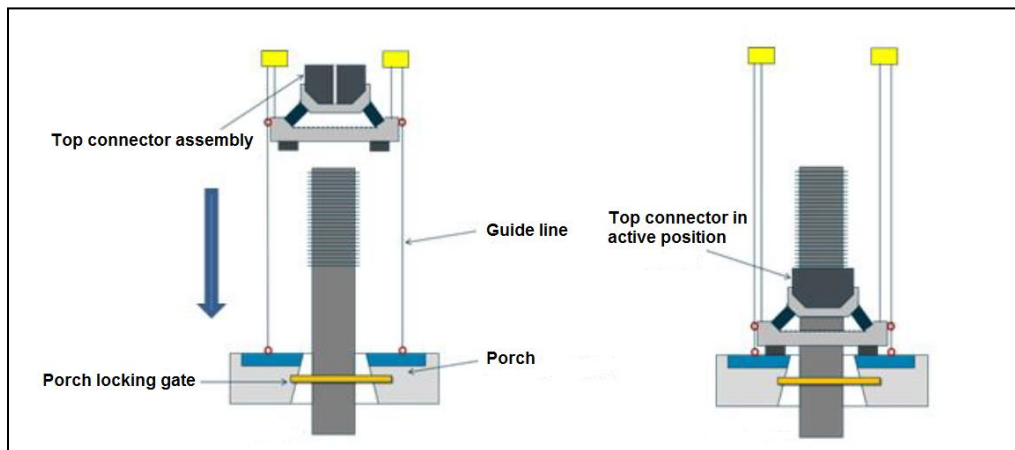
Figure 6.8: Tether connection configuration

After all the tethers have been locked and SFT parts have been de-ballasted, tether length adjustments are expected, to reach to the designed SFT configuration. This can be done with the use of specially developed tools named jacks. These tools when in position, take over the load from the top connector parts, allowing for adjustments on the position of the tether in order to reach the desired 10MN pre-tension on each tether.

Lastly, the buoyancy shafts are ready to be removed and corrosion caps to be placed around the tunnel-tether connection points.

6.4 Critical points and recommendations

In such big projects one small deviation from the plan can have disastrous consequences. It is crucial to plan everything thoroughly based on reasonable engineering knowledge. Some of the most important critical aspects of the installation procedure are mentioned here and many more can come up in a later phase:

- The tethers are planned to be installed prior to the tube installation. There will be a while that the tethers are going to be exposed to currents and waves. VIV's can make their presence and in combination with a long period of exposure, the fatigue life of the elements will significantly

reduce. An idea to tie the neighboring tethers together is proposed, which is not clear how much it can mitigate the effect.

- During the transportation of the tunnel, such a slender structure like an SFT is prone to bending moments. This can be caused by an incoming wave or even a current suddenly meeting the structure. How much the tunnel will react to an excitation like this depends on the restraining force from the tug boats. Further investigation is required.

- Another problem that arises in the transportation phase is the towing procedure. It needs to be clear that the points where the tug boats are connected, can withstand the pulling tension safely without damaging any part of the tube.

- During the tether hook-up its tether region is loaded individually, by de-ballasting the specific tube segment. This will lead to non-uniform displacements on the tube, which again will lead to stress variations along the length that need to be monitored. Moreover, deviations from the target tether lengths will cause different deformations and adjustments need to be made carefully.

The installation process of an SFT is a multivariable problem that needs detailed planning and design. Some aspects are briefly touched upon in the present report, but a more in depth approach is considered necessary.

7 Conclusions & recommendations

The main goal of the present thesis was to numerically analyze, evaluate and determine whether the submerged floating tunnel concept is technically feasible, regarding the environmental static and dynamic loading. The work has been divided into three main tasks, all contributing towards reaching the main objective. The most important conclusions of the report are summarized in section 7.1, and further recommendations for future development are found in section 7.2.

7.1 Conclusions

The first objective was to find an optimum set of angles for the tethers, in order to provide sufficient stiffness in supporting the tube. A set of $\alpha = 45^o$ and $\beta = 70^o$ (refer to Figure 3.1.a) is found to be the most suitable, taking into account all the possible limitations, while trying to stay in agreement with the prototype design developed by Norway. For this set of angles it was also found that modeling the tethers either using a linear or a non-linear approach doesn't affect the tunnel response (Appendix A). By applying linear springs with constant stiffness in modeling the tethers, saves both computational time and memory. Lastly, obtuse β angles are not suitable for restraining such a structure, as it was found that such a configuration leads to the amplification of the horizontal motions, due to the reduced rotational stiffness.

The second objective of the thesis was to model the complete 3D structure, under dynamic loading generated by a current flow of $1 \ ^m/_s$. The effect of VIV's on the tube was assessed, by calculating the vertical and horizontal oscillations. This was done, for varying number of tethers that support the structure. As it is expected, larger oscillations were observed in the vertical direction, caused by the vortex shedding behind the cylinder. VIV's start become significant for a configuration of 7 tether pairs or less. This corresponds to a free-span of $687m$, for an SFT of $15m$ diameter. From a simple estimation performed, swell waves don't seem to influence the structure more than the current flow previously investigated. The resultant forces from both 100 year current and swell wave were compared to justify this. Taking all the above into account, the prototype design is proven to be extremely robust to both the static and the dynamic loading coming from the marine environment.

The third objective was to test how the structure responds, when a tether unexpectedly fails. Can a chain reaction failure phenomenon be possible, leading to the complete structure failure? For the prototype design with 25 tether pairs, the answer is no. The structure can actively absorb the energy released, after the first unexpected failure, without any further system damage. This is not the case for tether configurations less than 24 pairs, though. A free-span of $220m$ or more will lead to a consequent tether failure. This is an undesirable phenomenon which has to be avoided.

Overall, the minimum number of tether pairs that needs to be used is 14, for the structure to stay in position, while loaded statically and dynamically. This corresponds to a free-span of $366m$, with a safety factor of 1.2 has been implemented.

No. Tethers		1	2	3	4	5	6	7	8	9	10	11	12	13	14	15	16	17	18	19	20	21	22	23	24	25
VIV non-sensitive		✗	✗	✗	✗	✗	✗	✗	✓	✓	✓	✓	✓	✓	✓	✓	✓	✓	✓	✓	✓	✓	✓	✓	✓	✓
Withstand static & dynamic Loads		✗	✗	✗	✗	✗	✗	✗	✗	✗	✗	✗	✗	✗	✓	✓	✓	✓	✓	✓	✓	✓	✓	✓	✓	✓
Chain reaction failure non-sensitive	Middle left tether fails	-	-	-	-	-	-	-	-	-	-	-	-	-	✗	✗	✗	✗	✗	✗	✗	✗	✗	✗	✓	✓
	Middle right tether fails	-	-	-	-	-	-	-	-	-	-	-	-	-	✗	✓	✓	✓	✓	✓	✓	✓	✓	✓	✓	✓

Table 7.1 summarizes all the SFT dynamic analyses performed, based on the developed model, showing each tether configuration capacities.

No. Tethers		1	2	3	4	5	6	7	8	9	10	11	12	13	14	15	16	17	18	19	20	21	22	23	24	25
VIV non-sensitive		✗	✗	✗	✗	✗	✗	✗	✓	✓	✓	✓	✓	✓	✓	✓	✓	✓	✓	✓	✓	✓	✓	✓	✓	✓
Withstand static & dynamic Loads		✗	✗	✗	✗	✗	✗	✗	✗	✗	✗	✗	✗	✗	✓	✓	✓	✓	✓	✓	✓	✓	✓	✓	✓	✓
Chain reaction failure non-sensitive	Middle left tether fails	-	-	-	-	-	-	-	-	-	-	-	-	-	✗	✗	✗	✗	✗	✗	✗	✗	✗	✗	✓	✓
	Middle right tether fails	-	-	-	-	-	-	-	-	-	-	-	-	-	✗	✓	✓	✓	✓	✓	✓	✓	✓	✓	✓	✓

Table 7.1: Sensitivity of the SFT based on the tethers used (✗: sensitive and ✓: non-sensitive)

Taking everything into account, the innovative concept of the submerged floating tunnel is challenging, but with lots of capabilities and potential. The developed model shows that such a structure can be constructed, safely operating, under certain constraints.

7.2   Recommendations

Several recommendations can be proposed for further research on the SFT concept, based on the present model. First and foremost, scale basin tests are necessary in order to prove that the concept is feasible. Furthermore, these tests will be used to calibrate the developed model and define an accurate set of tuning parameters for the wake oscillator. This will shed light on the assumption that was made, whether the known theory on VIV's for small diameter offshore structures can be up-scaled and used for large diameter cylindrical structures also. As a next step, the wave forces could be implemented, also, in the model, in parallel with the current forces. This would require special attention, though, as the two forces should be vectorially superposed[11].

Concerning a more accurate modeling of the SFT system, the tethers can be modeled as beam elements, instead of springs. VIV's are prone to happen in the tethers also, so the coupled motion of the tube and the tethers is of great interest. Apart from that, the bending of the tethers is ignored and it is unclear how much it would contribute to the tether loading.

---

[11] The quadratic drag force can lead to a significant underestimation of the resultant force, if one treats the two forces separately

8 Bibliography

1. **Paik.** *Analysis of wave force induced dynamic response of submerged floating tunnel.* s.l. : KSCE J.Civ.Eng., 2004.

2. **Mazzolani, Landolfo.R, Faggiano.B.** *Structural Analyses of the Submerged Floating Tunnel Prototype in Qiandao lake (PR of China).* 2008. 439-454.

3. **Hiroshi, Kunisu.** *Evaluation of wave force acting on Submerged Floating Tunnels.* s.l. : Procedia Eng., 2010. 99-105.

4. **Long.X., Wang.L.** *Effects of fundamental structure parameters on dynamic responses of submerged floating tunnel under hydrodynamic loads.* s.l. : Acta Mech., 2009. 335-344.

5. **Xiang.Y., Zhang.K.** *The layered integrating method for calculating wave force on submerged floating tunnel based on Morison equation.* s.l. : J. Zhejiang Univ. Eng. Sci., 2011. 1399-1404.

6. **Reinertsen, Olav Olsen.** *Bjornafjord Submerged Floating Tube Bridge.* 2016.

7. **Schack, Maria Hapnes von.** *Dynamic load effects on a submerged floating tube bridge with emphasis on vortex-induced vibrations.* s.l. : NTNU, 2017.

8. **Khalak.A., Williamson.C.H.K.** *Modes, Forces and mode transitions in vortex-induced vibrations at low mass-damping.* s.l. : Journal of Fluids and Structures, 1999. 214853.

9. **Facchinetti, Langre, Biolley.** *Coupling of structure and wake oscillators in vortex-induced vibrations.* s.l. : Journal of Fluids and Structures, 2004. 123-140.

10. **Reinertsen, Olav Olsen, Norconsult.** *Bjornafjord Submerged Floating Tube Bridge.* 2016.

11. **Chandler.B.D., Hinwood.J.B.** *Combined wave-current forces on horizontal cylinders.* 1982.

12. **Petterson.H., Kahma.L.**

13. **Barbosa.M.O.J., Qu.Y.,Metrikine.V.A.,Lourens.E.M.** *Vortex-induced vibrations of a freely vibrating cylinder near a plane cylinder: Experimental investigation and theoretical modeling.* Delft : Journal of Fluids and Structures, 2017.

14. **Xiang.Y., Yang.Y.** *Challenge in design and construction of submerged floating tunnel and state-of-art.* Hangzhou : Elsevier Ltd., 2016.

15. **Naik.M., Zahid.U.** *Performance evaluation of submerged floating tunnel subjected to hydrodynamic and seismic excitations.* Hanyang : Applied Sciences, 2017.

16. **Naik.M., Zahid.U.** *Performance evaluation of submerged floating tunnel to hydrodynamic and seismic excitations.* Hanyang : Applied Sciences, 2017.

17. **Xiang.Y., Yang.Y.** *Spacial dynamic response of submerged floating tunnel under impact load.* Hangzhou : Marine Structures, 2016.

18. **Chen.Z., Xiang.Y.,Lin.H.,Yang.Y.** *Coupled vibration analysis of submerged floating tunnel system in waves and current.* Hangzhou : Applied Sciences, 2018.

19. **Sarpkaya.T.** *Hydrodynamic forces from combined wave and current flow on smooth and rough circular cylinders at high reynolds numbers.* Houston, Texas : Naval postgraduate school, 1984.

20. **Journee.J.M.J., Massie.W.W.,Huijsmans.R.H.** Wave forces on slender structures. *Offshore Hydromechanics.*

9 Appendix A

9.1 Comparison of Linear (Blue) and Non-Linear (Red) response on a 2D static analysis